Journal of Manufacturing Processes 143 (2025) 132–150

Contents lists available at ScienceDirect

Journal of Manufacturing Processes

journal homepage: www.elsevier.com/locate/manpro

Quasi-industrial accelerated testing of a HIPIMS deposited nano-layered CrAlYN/CrN coating for improving hot forging die life of nitrided H13 steel

Christopher Fleming [a,*], William Kerr [a], Bhaskaran Krishnamurthy [a], Liza Hall [a], Arunprabhu Sugumaran [b], Arutiun Ehiasarian [b], Papken Hovsepian [b]

[a] Advanced Forming Research Centre, The Department of Design, Manufacture and Engineering Management, University of Strathclyde, 85 Inchinnan Drive, Inchinnan, Renfrewshire, PA4 9LJ, United Kingdom

[b] National HIPIMS Technology Centre, Sheffield Hallam University, Howard Street, Sheffield S1 1WB, United Kingdom

ARTICLE INFO

Keywords:
Hot forging
Tool life
Wear resistant coating
HIPIMS
Nitriding
H13 steel

ABSTRACT

Die life is a major concern in the hot forging sector because of ramifications for productivity and costs. Despite surface engineering technologies being an established route to protecting against die surface degradation, to the authors' knowledge there are no reports of a high-power impulse magnetron sputtering (HIPIMS) deposited coating having been trialled for this purpose. In this study, a 0.8 μm thick CrAlN base layer followed by a 9.0 μm CrAlYN/CrN nanoscale multilayer was deposited via HIPIMS onto a HIPIMS-pretreated nitrided H13 tool steel. The comparator was nitrided H13. An accelerated test method employed an industrial-scale screw press to forge 260 Inconel 718 billets onto a model die that was designed to exacerbate susceptibility to damage. Billets were preheated to 1000 °C and the tools were held at 250 °C. These conditions were sufficient to induce in the nitrided only die many of the damage mechanisms that variously determine real-world hot forging tool life. In contrast, the coating did not suffer abrasive wear or thermomechanical fatigue cracking and was considerably more resistant to oxidation and pick-up. Additionally, the coating provided excellent thermal insulation of the substrate and, hence, protection against thermal softening-induced plastic yield. It did not, however, protect against mechanical fatigue, with cracks occurring in the same single region of both dies. Although these led to localised complete loss of coating, the substrate was protected until such point and the onset of wear was significantly delayed.

1. Introduction

Deterioration of die surface condition over the course of a metal forming production run will ultimately necessitate stoppage for changeover. In addition to the downtime that this entails, resources are required to repair the worn die set and rework out of tolerance components. In extreme cases, dies and components will be scrapped. Ramifications in terms of yield and expenditure can be significant. These effects are especially keen with hot forging, where the financial burden can be as high as 30 % of production costs [1]. Consequently, any material that can increase damage resistance beyond that of the state of the art can potentially have huge benefits.

With hot forging, die damage can occur via many mechanisms. These include mechanical fatigue, thermomechanical fatigue (TMF), plastic deformation, abrasion, adhesion, spallation and tribochemical phenomena. The latter four are associated with progressive material loss and in accordance with DIN 50323 are often collectively referred to as wear [2]. All these mechanisms originate at the surface or near-surface region; consequently, die surface treatments are an established route towards protecting against them. Amongst many such technologies, the combination of a nitrided layer with a physical vapour deposition (PVD) or plasma assisted chemical vapour deposition (PACVD) coating (variously known as a duplex or hybrid treatment), has emerged as one of the most effective. The nitrided layer increases substrate resistance to plastic deformation and cracking and protects the coating from loss of cohesion and adhesion. The coating protects the nitrided surface from abrasion and thermal effects and may also reduce friction.

High-power impulse magnetron sputtering (HIPIMS) technology can enable PVD coatings with enhanced adhesion, superior density, and higher toughness [3]. Benefits are especially pronounced when HIPIMS is used for both pre-treatment and coating deposition, i.e. the HIPIMS-HIPIMS technique. Despite having been reported upon since the late

* Corresponding author.
E-mail address: christopher.fleming@strath.ac.uk (C. Fleming).

https://doi.org/10.1016/j.jmapro.2025.03.106
Received 20 June 2024; Received in revised form 17 February 2025; Accepted 26 March 2025

1990s [4], to the authors' knowledge there are no published works concerning the use of HIPIMS coatings as a means of protecting hot forging dies. This work is an investigation into the potential of a duplex treatment of nitriding and a CrAlYN/CrN nanoscale multilayer coating deposited by the HIPIMS-HIPIMS technique for this purpose.

The various hot forging die damage mechanisms rarely occur in isolation, they typically exhibit strong local intensity variations within a process, and the dominant reason for failure is often process specific [5]. It thus follows that the most reliable method of evaluating the performance of a surface treatment in terms of a particular process is to trial it in production [6]. New technologies, however, bring with them a risk of adverse outcomes. And in a forging facility, preservation of output typically takes precedence. It is therefore necessary that methods exist by which to first both ascertain potential benefits and derisk.

At what could be considered the opposite extreme from production trials are laboratory-scale tribometers that feature idealised contacts. Conventional devices were typically developed to study closed-system mechanical applications such as bearings and gears and are limited in terms of reproducing metal forming contact conditions. Thus, research groups operating in this field often build bespoke apparatus. The *warm and hot upsetting sliding test* has been used to evaluate the protection offered by graphite and 'white' lubricants against abrasive wear [7], and by sol-gel tool coatings against abrasive wear and adhesive wear [8]. Using the *plane strain hot forging wear test*, different die surface treatments were assessed in terms of susceptibility to tempering, fracture, oxidation, and spallation [9]. A test rig at Karlstad University, Sweden has been used to study the thermal fatigue susceptibility of a range of surface engineered hot work tool steel systems [10], and a TMF test rig at the University of Padua, Italy was specifically designed to simulate hot forging conditions [11]. Whilst valuable insight has undoubtedly been gained by such methods, they fail to recreate the real-world superposition of damage modes.

Occupying the middle ground between production trials and laboratory-scale tribometers is the use of a real press and industrially relevant process parameters to forge billets between a model die set. This approach requires multiple equivalent dies to be fabricated, with each undergoing a different surface treatment. Evaluation of performance is via comparative assessment of the deterioration of surface condition [12]. To draw analogy with the distinction made by Bay et al. concerning sheet metal forming tribotests [13], these may be considered process tests cf. simulative tests in the preceding paragraph. Despite the advantages of this approach, there are few examples in the literature. This may be because it is uncommon for a research centre to have access to an industrial-scale press. It may also be because thousands of forging cycles can be necessary for appreciable performance differences to be revealed [14], thereby rendering trials prohibitively expensive.

For this study, the first factor was not an issue because the Advanced Forming Research Centre has industrial-scale forging presses on site. To mitigate the second, a die was designed to accelerate incurrence of damage and the nickel-base superalloy Inconel 718 (IN718) was selected as the billet material. Previous assessments of duplex-treated hot forging dies have almost entirely involved medium carbon steel billets, including AISI 1043 (DIN C45) [15], AISI 4130 (DIN 25CrMo4) [16] and AISI 4140 (DIN 42CrMo4) [12]. At 1000 °C, IN718 flow stresses can be three times those of a medium carbon steel [17]. Consequently, die life is often measured in hundreds rather than thousands of parts and is a major problem [18]. This is especially true with precision forging which demands close tolerances, small radii and high-quality surface finish. An additional benefit of establishing performance in terms of this alloy is augmentation of the importance of results with respect to high-value manufacturing. This is because forged IN718 components are extensively used within the aerospace and energy industries [19,20].

This paper commences with the results of a finite element (FE) simulation created to gain insight into the temperatures and mechanical stresses generated at the surface of the test die during the forging operation. Then, after describing the virgin condition of a duplex-treated (nitriding followed by CrAlYN/CrN HIPIMS coating) and a nitrided only comparator die, a comprehensive comparative assessment of the post-forging conditions is made. Results indicate that protection afforded to hot forging dies by the novel surface treatment may be considerable and multifaceted.

2. Experimental

2.1. Die design

Fig. 1 shows Solidworks CAD models of the die and the assembly within the press. The basis of operation is that a cylindrical billet is positioned onto a recessed seat and up against an end stop. The billet is then forged onto a trapezoidal prism under impact by a planar upper die. To maximise material utilisation, the design features two such prisms, thereby enabling two sets of trials to be conducted using a single machined block, simply by rotating it through 180° in the press. The front and rear faces and edges can in principle be manufactured to any angle and radius of curvature, respectively, to offer flexibility of contact conditions. In the configuration used in this study, the front and rear planes were at 45° and 22.5°, respectively, to the normal and the corresponding edges were machined to a 1 mm and 2 mm radius, respectively. All other edge rads had 1 mm curvature.

2.2. Materials and treatments

A DMG Mori HSC 75 precision machining centre was used to produce the die from a 105 × 75 × 50 mm block of H13 hot work tool steel that had been vacuum hardened and fluid bed double tempered to give a hardness of 53 HRC (Cogne UK Ltd., Sheffield, UK). IN718 workpieces were supplied as cylindrical billets (Ø = 25 mm and length = 50 mm) that had undergone a typical annealing and aging cycle (Righton and Blackburns Ltd., Glasgow, UK). Upon receipt, the billets were solution-treated at 1040 °C for 1 h followed by a water-quench. The supplier-stated compositions of the die and workpiece alloys are given in Table 1.

Die forging surfaces were polished to a nominal 0.08 μm Ra and plasma nitrided by Wallwork Cambridge Ltd., UK. Parameters were typical of a commercial process, with $T = 510$ °C and $t = 8$ h. A compound layer is brittle and can be detrimental to coating retention so was removed via a second round of polishing, again to a nominal 0.08 μm Ra. The remaining diffusion zone contains a fine dispersion of coherent or semi-coherent nitrides of the alloying elements [21], and enhanced hardness for H13 has been attributed chiefly to the presence of CrN precipitates [22]. Up to this point, both die impressions were prepared equivalently.

One prism was then masked off and a CrAlYN/CrN nanoscale multilayer coating was deposited on the other using an industrial-size (chamber volume = 1 m^3) Hauzer 1000-4 system at the National HIPIMS Technology Centre at Sheffield Hallam University, UK. In the first step of the process, the specimens were pre-treated with high-voltage electrical biasing and immersion in a highly ionised plasma containing Cr^+, Al^+, Y^+ and Ar^+ ions generated by a HIPIMS plasma discharge sustained on a CrAlY target. Energy-resolved mass spectroscopy of the HIPIMS plasma demonstrated strong fluxes of Cr^+ ions and significant presence of double ionised Cr^{2+} species. The HIPIMS pre-treatment leads to a surface that is extremely clean and free of native oxides, with good crystallinity, and free of macroparticles. Thereby providing conditions for local epitaxial growth of the coating over large surface areas [23]. In the next steps, a 0.8 μm thick CrAlN base layer followed by a 9.0 μm CrAlYN/CrN nanoscale multilayer was deposited using a combined technique of unbalanced magnetron sputtering and HIPIMS. Typical deposition temperature was 450 °C. Low-angle X-ray diffraction revealed the superlattice structure of the coating with bilayer thickness = 8.4 nm. Adhesion was excellent of class HF-1 when determined by the Rockwell C indentation (Daimler Benz) test [24].

The microstructure and mechanical properties of this coating have

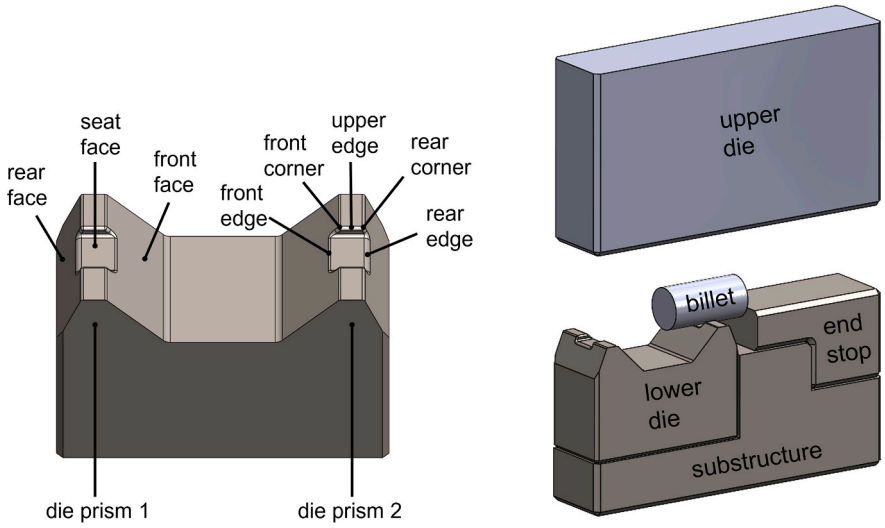

Fig. 1. CAD models of (left) the lower die labelled with regions of interest, and (right) the assembly within the forging press.

Table 1
Supplier-stated wt.% compositions of the die and billet alloys used in this study.

	Fe	C	Si	Mn	P	Cr	Mo	Ni	Cu	Co	Ti	Al	Nb	V
H13	Bal	0.37	1.03	0.38	0.02	5.09	1.26	–	–	–	–	–	–	0.91
IN718	Bal	0.02	0.11	0.13	0.01	19.29	3.09	53.27	0.02	0.01	1.01	0.55	5.28	–

been comprehensively described previously [25,26]. The structure was columnar, individual columns terminated at the surface in a dome-shape, and boundaries were very dense on account of the use of a highly ionised deposition process. The preferred crystallographic orientation was (220). Room temperature nanoindentation hardness measurements showed a hardness of 28 GPa and elastic modulus of 384 GPa.

2.3. Testing procedure

Forging trials were performed using an industrial scale 2100 kN Schuler screw press. The press energy was set at 8 % (12.8 kJ) and the upper tool velocity was 200 mm s^{-1} at the point of initial contact and 155 mm s^{-1} at the end of forging. The upper and lower dies were held at 250 °C. Billets were heated to 1000 °C in an Electrotherm rotary furnace with a minimum soak time of 15 min. A forging cycle comprised manually spraying the die prism under investigation with a 5 wt% graphite in water suspension (James Durrans W1010), manually transferring a billet from the furnace to the recessed seat, and then setting the press into motion. This was repeated for each billet and 260 billets were forged onto each of the nitrided and nitrided/HIPIMS coated die prisms (hereafter referred to as the N-die and N+HIPIMS-die, respectively). The mean transfer time was 3.3 ± 1.0 s, and the mean dwell time was 2.9 ± 0.5 s. It should be noted that glass billet coatings tend to be used in industry when forging IN718. These coatings present a thermally insulating barrier that protects against workpiece cooling and die heating, inhibits workpiece scale formation, and can reduce friction. With the intention of exacerbating die degradation, no such coating was used here.

2.4. Analysis procedure

The virgin and post-forging surface conditions of the dies were captured using an Alicona InfiniteFocus G4 focus variation optical profilometer. Areal surface texture evolution was evaluated using the amplitude parameters Sq (root mean square height) and Sz (maximum height), the feature parameter S10z (ten-point height) and the hybrid parameter Sdq (root mean square gradient). Measurements were made from the primary dataset, i.e. with only nominal form and the smallest scale elements removed (the so-called areal S-F surface [27]). For each region investigated, mean parameter values were calculated from three image fields that each spanned the breadth of contact.

Higher magnitude imaging and elemental analysis were performed using an FEI Quanta 650 field-emission scanning electron microscope (SEM) equipped with Oxford Instruments Aztec energy dispersive spectroscopy (EDS) capability. All given EDS results were normalised to 100 % and carbon counts were excluded to prevent organic surface contaminants and possibly residual graphite from skewing findings.

The geometries of the pre- and post-forging dies and of selected forged billets were captured using a GOM ATOS Triple Scan non-contact 3D scanner. A thin layer of talc was applied to specimens to minimise surface reflections. Using GOM Inspect software, corresponding before and after die surface meshes were overlaid and best fitted and a colour map was generated showing height differences between the two states. A similar approach was adopted for the billet scan data, except each was overlaid with the first in the run.

To compute volume differences, meshes were split into regions of interest, regularised, and then imported into MATLAB. For each mesh, the vertices were extracted and a meshgrid was created using the XY extremities. A modified version of the ‘griddata’ function was used to produce an interpolated grid of points across equidistant XY co-ordinates. All data within the outer 0.5 mm in the X and Y axes was then removed because the original data was often jagged in these regions. This resulted in point clouds for a given die/billet region with identical XY coordinates. For each comparison, the ‘before’ Z data was subtracted from the ‘after’ to generate a height difference map. By multiplying the values of a map with the XY resolution of the meshgrid and then summing, the volume difference between two samples was calculated.

Once top-down analysis was complete, the samples were sectioned in the longitudinal direction. First, they were polished to 1 μm using diamond paste and microhardness depth profiles generated using a Mitutoyo MicroWhizHard Knoop micro-hardness tester and a 0.25 N load.

Measurements were taken at the surface and at intervals of 50 μm to a depth of 400 μm. The cross-sectioned samples were then etched with 2 % Nital solution to reveal the nitride layer, and examined using Leica DM12000M optical microscope and SEM/EDS. To obtain baseline measurements, i.e. the dies in the virgin condition, microhardness and microscope analyses were also performed on H13 blocks that were nitrided/duplex-treated at the same time as the dies.

2.5. FE simulation

To gain insight into the temperatures and mechanical stresses affecting the surface of the test die during the forging operation, an FE simulation and analysis was carried out using the commercial metal forming software QForm.

Input H13 flow stress data was obtained from elevated-temperature tensile tests conducted according to the ASTM E21 standard using a Zwick Z250 standard testing machine equipped with controlled heating chamber. Specimens were machined as per the ASTM E8/E8M standards from the same batch of H13 used for manufacturing the dies. Tests were performed at 250 °C, 350 °C, 450 °C and 550 °C and at strain rates of 0.001 s^{-1} and 0.1 s^{-1}. Note that although a preliminary simulation indicated a maximum die surface temperature of >700 °C, tensile tests could not be performed above 550 °C due to risk of platen deformation. The load-displacement data obtained from the tensile tests was converted to true stress–true strain data using the standard method, and from this yield stress versus temperature values were calculated. Supplementary thermal and mechanical properties of H13 and all IN718 properties were sourced from the literature [28].

A fully coupled 3D thermomechanical FE simulation of a single forging operation was carried out with process conditions equivalent to those in the physical operation (Section 2.3). The lower die and billet were made elastic-plastic, and all other components were treated as rigid. A fine tetrahedral mesh (0.5–1 mm) with remeshing option enabled was employed in the contact region. The Levanov friction model

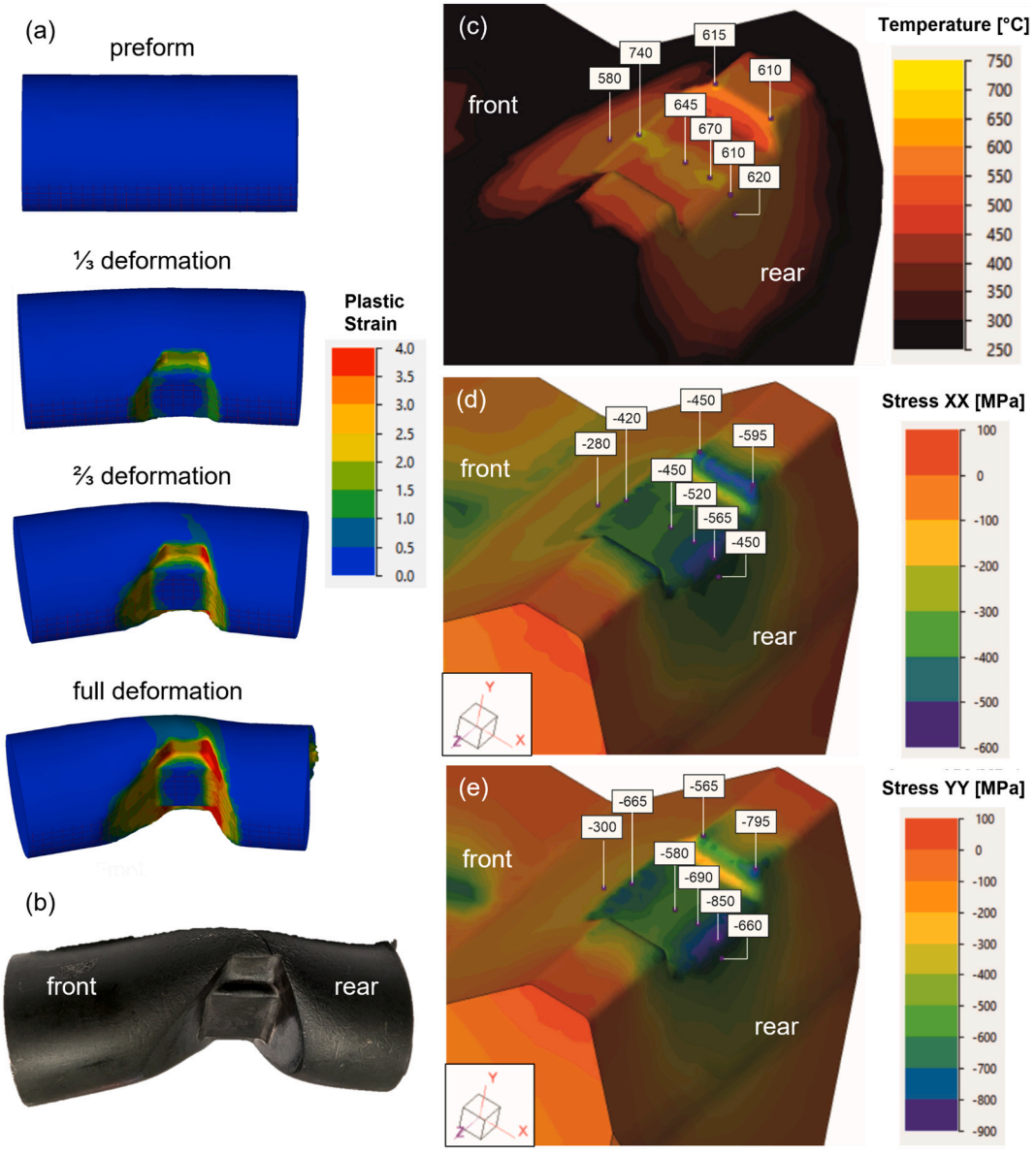

Fig. 2. (a) Finite element models of the billet at selected successive stages of the forging operation that are colour-mapped to degree of plastic strain. (b) Photograph of a fully forged billet. Finite element analysis estimated distributions of (c) surface temperature, (d) horizontal stresses, and (e) vertical stresses across the die at the end of a single forging operation. The annotations display the magnitude and position of the maximum in each region (as labelled in Fig. 1) as well as that in the centre of the seat face.

was used with the friction factor set at 0.4 and the Levanov coefficient at 1.25, as per QForm recommended inputs for hot forging of nickel-alloys. The heat transfer coefficient between the workpiece and dies was taken to be 22,500 W m^{-2} K^{-1} [29]. Ambient air was assumed to be at 20 °C and a convective heat transfer coefficient of 30 W m^{-2} K^{-1} was used. An emissivity value of 0.6 that is typical of nickel-alloys under hot forging conditions was used for calculation of radiative heat loss. Coefficients for the transformations of deformation energy and friction into billet thermal energy were set at 0.95 [30]. Validation was by way of comparison with press load data and final geometry.

3. Results and discussion

3.1. FE simulation

Fig. 2(a) shows FE models of the billet at selected successive stages of the forging operation that are colour-mapped to degree of plastic strain. Beneath this, Fig. 2(b), there is a photograph of a fully forged billet to enable comparisons.

Fig. 2(c) shows the numerically estimated temperature distribution across the surface of the model die at the end of a single forging operation. The maximum reached on each face, edge, and corner was variously between 580 and 740 °C. A consequence of the contact time between workpiece and die being so short (≈260 ms) is that only the uppermost surface layer reaches these values, and temperatures drop sharply to that of the bulk, i.e. 250 °C, with depth.

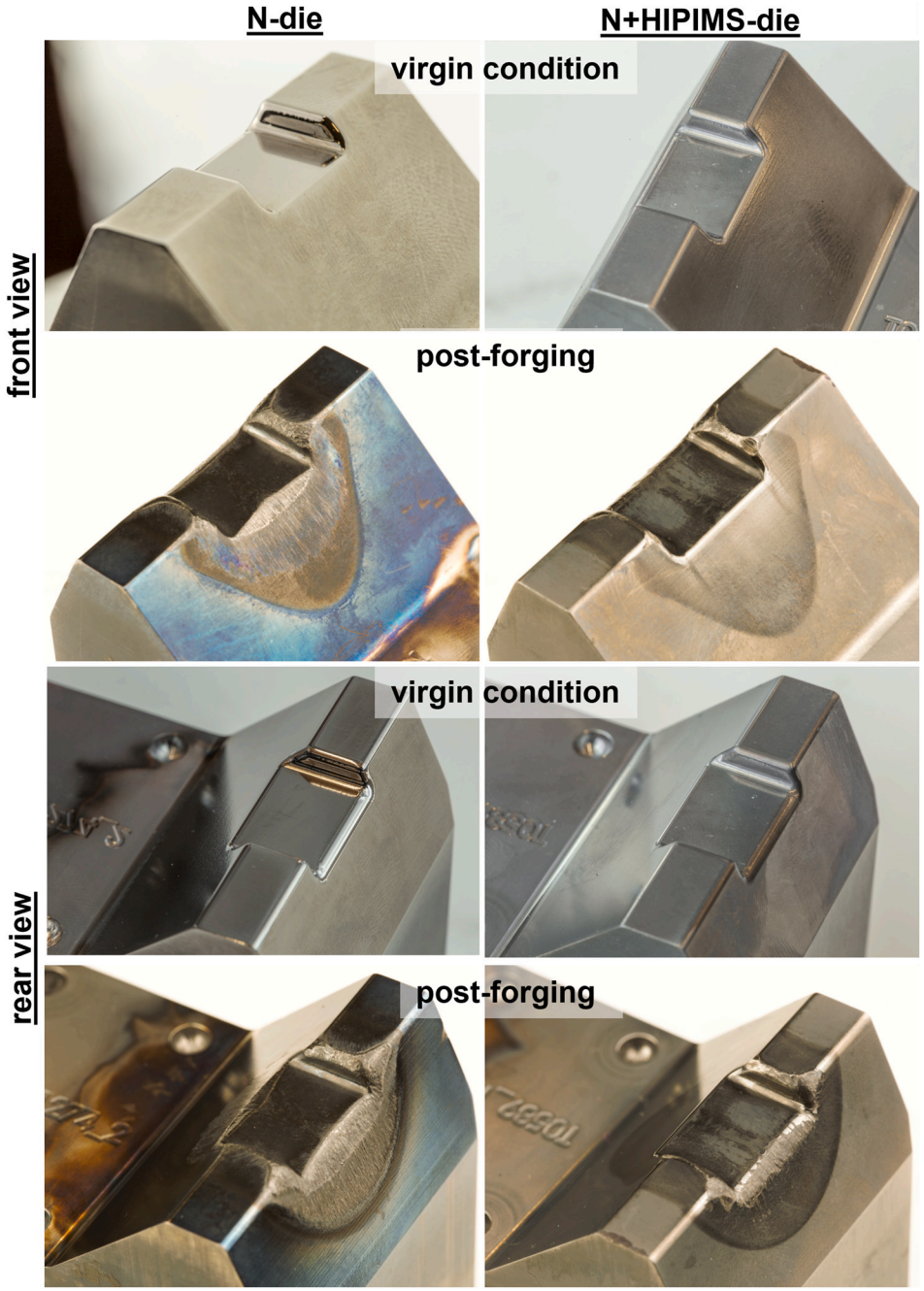

Fig. 3. Photographs showing the pre- and post-forging conditions of the two dies from front and rear viewpoints.

Similarly, numerically estimated values of mechanical stresses in the orthogonal X (horizontal) and Y (vertical) directions are shown in Fig. 2 (d) and (e). That the values over the contact region are all negative indicates universally compressive stresses. The maximum stresses reached at each region exhibited greater spread than the temperatures, ranging from 280 to 595 MPa in the X direction and from 300 to 850 MPa in the Y.

A further key outcome is that mechanical stresses were predicted to be considerably greater at the rear of the die than the front. This difference principally stems from physical constraints imposed by the end stop part of the assembly. At the front, the billet is constrained only in the upwards direction by the active loading of the upper die and in the back direction by reaction forces at the lower die front face and is free to move in all other directions. At the rear, the billet is constrained from three sides by the upper die, lower die rear face and the end stop and so has more limited freedom of movement. This introduces higher normal stress as well as shear stresses at the interface between billet and lower die. Crucially, as will be shown in subsequent sections, this finding manifested in the physical trial wear patterns.

To conclude this section, it should be made clear that the estimated temperatures and stresses apply only to the first cycle and will change over the course of a run due to cumulative effects and as wear alters local geometry. Furthermore, the simulation did not include a nitride layer. Therefore, whilst the outputs in absolute terms should be considered with some reservation, they nonetheless provide insight into how each die region is affected by workpiece contact and help rationalise spatial variations of specific damage modes.

3.2. Pre-forging condition

Photographs of the front and rear of the N-die and N+HIPIMS-die in the virgin condition are shown in Fig. 3. The sole macroscopic difference between the two was a dissimilarity in colour, with the coated die having exhibited a slightly darker lustre. The typical surface condition of each is shown in the Fig. 4 optical profilometry images and areal texture results are given in Fig. 18. The texture that can be seen is from the post-nitriding polishing, and as such is superficial. That it remains apparent after coating exemplifies just how closely the HIPIMS technique follows substrate surface features. Key findings from areal texture analysis were that in terms of Sq, the HIPIMS coating did not affect the surface texture of any of the three faces. According to Sz, S10z and Sdq, however, it did; increasing each by a factor of between 1.8 and 3.2, 1.5–2.6 and 1.7–1.8, respectively, depending on the face. This exemplifies the importance of using multiple parameters when evaluating surface texture. From inspection of optical profilometry images, these differences may in part be attributed to shallow depressions that punctuated the surface of the coated substrate. These are fairly common with PVD coatings and are typically sites where dust particles that had settled on the surface were ejected during growth. Of further note is that for each die, the front and rear faces were equivalent in terms of Sq, Sz and S10z and rougher than the seat face according to these metrics by factors variously ranging from 1.4 to 2.8. The three faces of each die were equivalent according to Sdq.

3.3. Post-forging condition

3.3.1. Macroscale visual evaluation

It was immediately apparent from visual inspection of the post-forging dies that the HIPIMS coating had imparted remarkable protection to the nitrided substrate. This can be appreciated from comparison of the Fig. 3 photographs. With the N-die, both the front and rear edges appeared to have been flattened. Furthermore, these edges and the corresponding faces were all textured in a manner indicative of heavy abrasion. In stark contrast, there was no discernible wear to the front edge or front face of the N+HIPIMS-die, and the sole features evident on the rear face were a few short, faint lines extending down from the edge. The rear edge on the other hand had suffered loss of form and was punctuated by pronounced grooves that ran parallel to the sliding direction. There was no visible damage to the seat face of either die. Whilst the four corners of both dies had been damaged out of existence, the connecting upper edges of the N-die were considerably more marked and deformed than those of the N+HIPIMS-die.

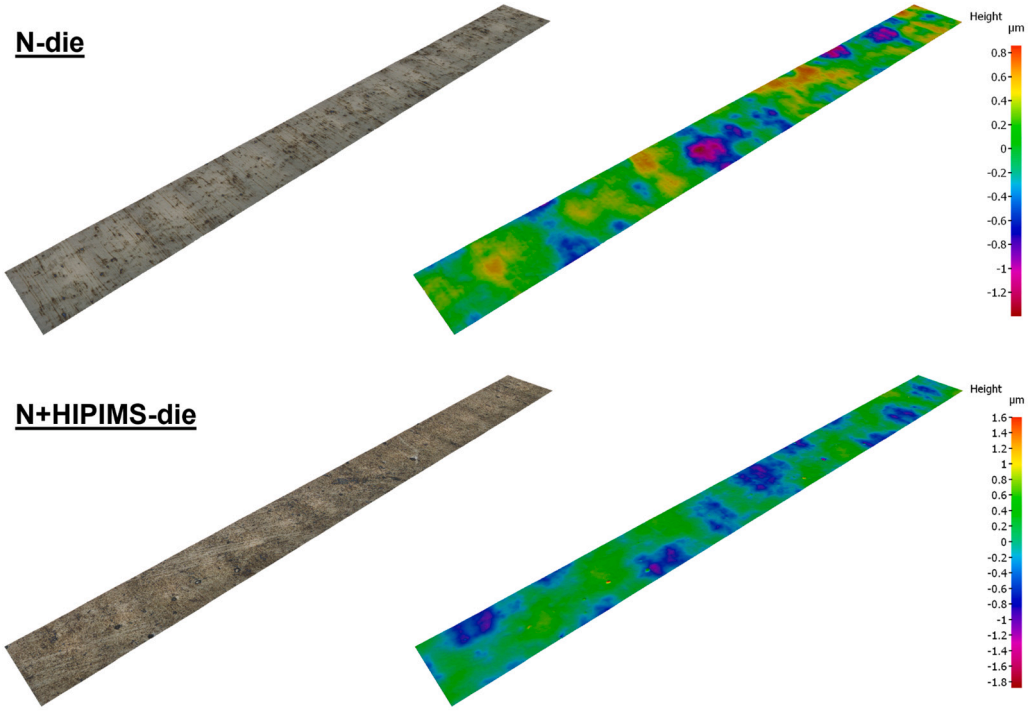

Fig. 4. True-colour and pseudo-colour optical profilometry images showing a typical region of virgin surface of the N-die and N+HIPIMS-die. All sites on each respective die were qualitatively equivalent and quantitatively similar and that shown was taken from the front face. Image field dimensions are 1.36 × 0.15 mm.

3.3.2. Microscale analysis

3.3.2.1. Edges. Optical profilometer image fields that covered the apex of the front and rear edge radii (or where appropriate, the location where the apex would have been) agreed with the macroscale observations. This data is shown in Fig. 5. Corresponding top-down SEM micrographs and EDS results and cross-section optical micrographs are shown in Fig. 6 for the front edges and Fig. 7 for the rear edges. Note that it was not possible to perform these analyses on the upper edges due to geometrical constraints.

In the case of the N-die, both the front and rear edges were covered in deep grooves, with those on the rear edge considerably broader than those on the front. The underlying form of the entire front edge was planar, as was much of the rear edge around where the apex had been. No nitride layer was evident at either edge. A network of TMF cracks was observed over part of the front edge and none were apparent on the rear edge. In contrast, uniaxial and parallel mechanical fatigue cracks orientated in the direction of workpiece flow had formed on the rear edge (Fig. 8) and not the front. These different susceptibilities towards fatigue types are in accordance with the FE simulation that indicated the highest surface temperature occurred at the front edge and the highest mechanical stresses at the rear edge.

Further to H13 alloying elements, top-down elemental analysis detected a high proportion of oxygen (30–35 at.%) and appreciable quantities of IN718 alloying elements (e.g. nickel ≈3.0 at.%). This indicates a susceptibility of nitrided H13 to oxidation and pick-up under process conditions. Post-sectioning, only patches of oxide layer remained adhered at either of these two sites and it was consistently between 2 and 5 μm thick.

Turning attention to the N+HIPIMS-die, top-down elemental analysis indicated that the coating had completely gone from the rear edge. This was confirmed with microscopy of the cross-section. Whilst abrasion marks in the exposed substrate were clear, they were less pronounced than on the corresponding edge of the N-die. Furthermore, the flattened section where the apex had been was much shorter, and remnants of nitride layer existed at the extremities with the thickness tapering off considerably less abruptly. As with the N-die, periodic longitudinally orientated mechanical fatigue cracks had formed at this edge. However, the cracks appeared both less numerous and broader with this die. That they exactly spanned the exposed region indicates that this cracking was either the cause or initiator of coating removal. Remarkably, no signs of abrasion, loss of curvature, cracking or coating loss were evident at the N+HIPIMS-die front edge.

The oxygen content of the exposed rear edge near-surface region was comparable to that of the N-die front and rear edges, and the amount of adhered IN718 was less by a factor of approximately two. Appreciable levels of silicon above that expected from the two alloys along with magnesium and sodium were detected at this edge (as well as on the seat face of both dies) indicating the presence of surface contaminants. Although the source is unknown, they undoubtedly originated through the forging operation and EDS mapping showed them to be associated with high levels of oxygen. Thus, the extent of die oxidation that occurred at this edge was not as great as the detected oxygen would suggest. Oxide layer that survived the cross-sectioning procedure had a thickness of between 2 and 4 μm. The oxygen content at the front edge was very slight (<2 at.%), no oxide layer was observed via cross-section analysis, and no pick-up was detected.

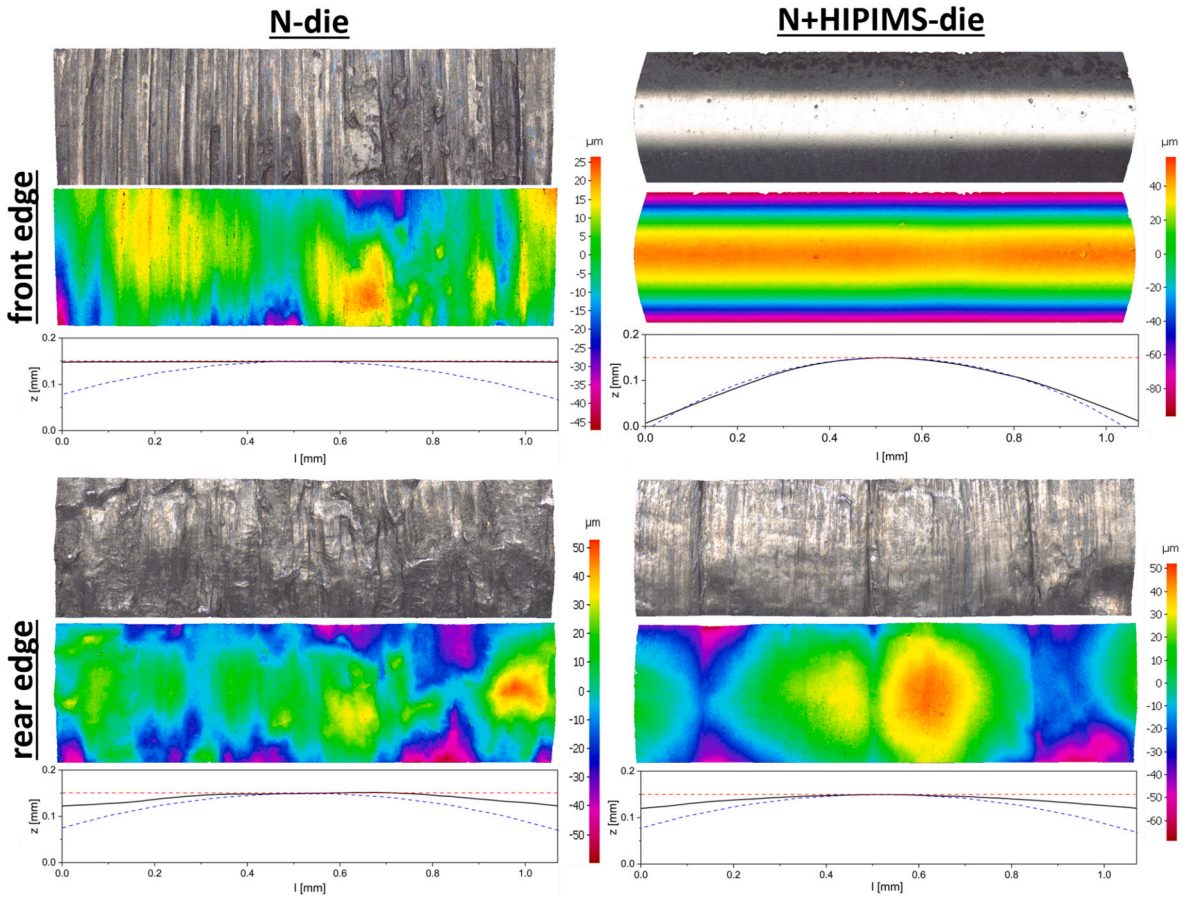

Fig. 5. True-colour and pseudo-colour optical profilometer images showing typical regions of the front and rear edges of the post-forging N-die and N+HIPIMS-die. Also shown are the mean line profiles from each region. To guide the eye, alongside are plotted a straight line and an arc of radius equal to that of the edge in the virgin condition, i.e. 1 mm or 2 mm. Image field dimensions are 3.94 × 1.09 mm.

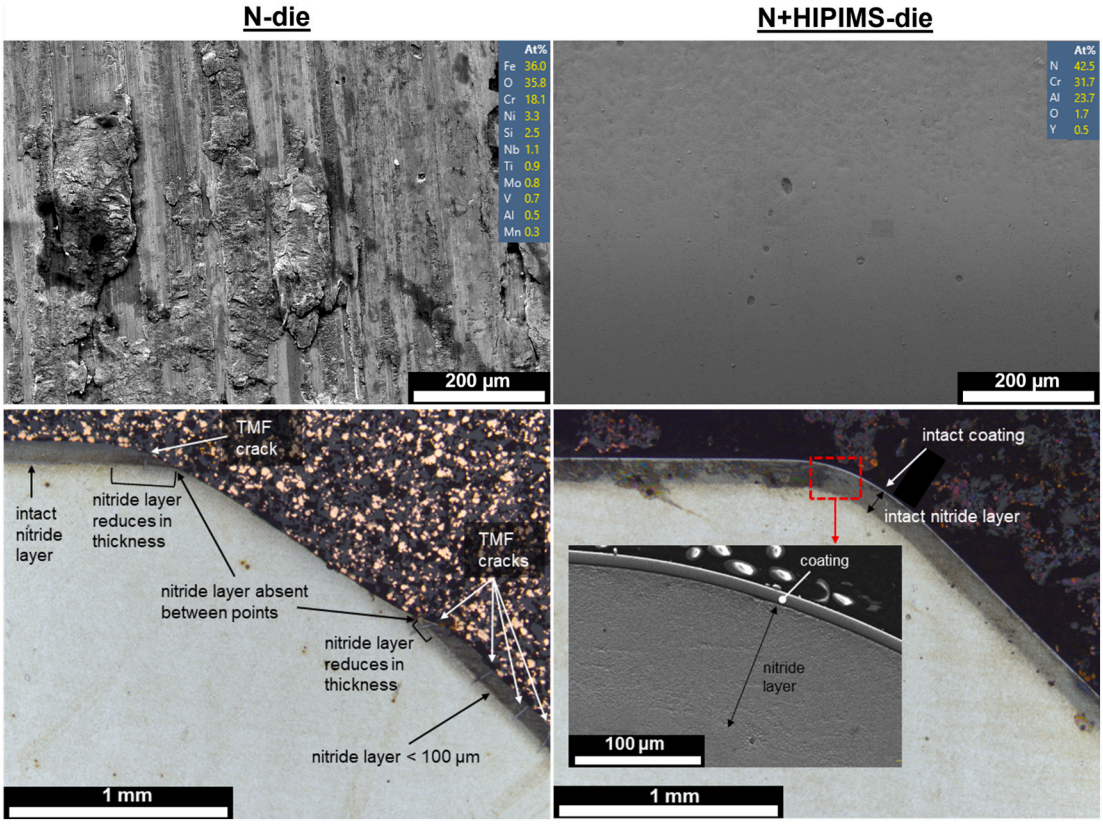

Fig. 6. (Top) SEM secondary electron images showing the typical surface of the front edge of the post-forging N-die and N+HIPIMS-die. The insets are the EDS determined elemental compositions. (Bottom) Optical micrographs of the full cross-section of the front edge of each die. The inset to the N+HIPIMS-die image is a higher magnification SEM secondary electron image showing the coating to be intact at the apex.

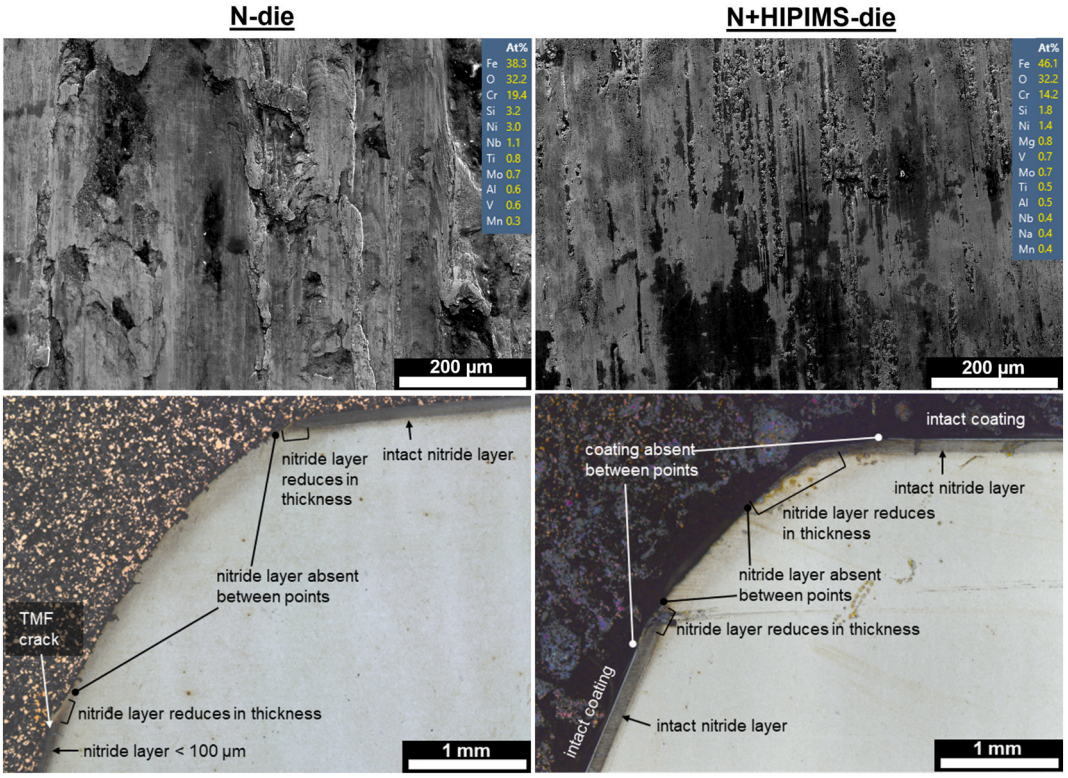

Fig. 7. (Top) SEM secondary electron images showing the typical surface of the rear edge of the post-forging N-die and N+HIPIMS-die. The insets are the EDS determined elemental compositions. (Bottom) Optical micrographs of the full cross-section of the rear edge of each die.

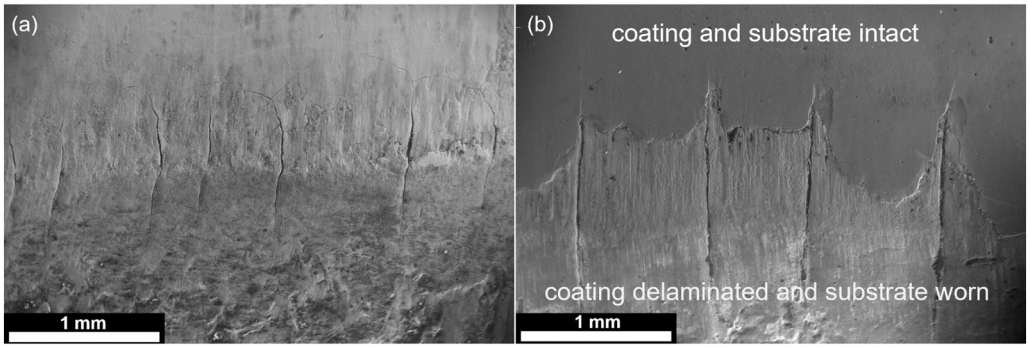

Fig. 8. SEM secondary electron images showing mechanical fatigue cracks at the rear edge of the post-forging (a) N-die and (b) N+HIPIMS-die.

3.3.2.2. Faces. Optical profilometer, top-down SEM/EDS, and cross-section SEM data underpinning this section are shown in Figs. 9, 10, and 11, respectively.

As was observed on the macroscale, much of the N-die front and rear face contact regions were covered in vertically orientated features indicative of abrasion. The rear face was significantly worse affected than the front according to all measured surface texture parameters (Section 3.3.4 and Fig. 18); a difference that is in accordance with the FE simulation that showed stresses to be greater at the rear. Clear from both SEM and optical microscopy were a network of cracks on each face typical of TMF (Fig. 12). The horizontally orientated cracks were generally periodic, and each spanned the breadth of the contact zone. In contrast, the vertically orientated cracks were irregular and short. Such a "rectangular-type" pattern is indicative of a bi-axial stress state that is dominant in one direction [31]. These cracks penetrated through the full thickness of nitride case depth and terminated a short distance into the bulk (Fig. 11(a)).

At 25–30 at.%, the oxygen content of the near-surface region of the front and rear faces was high, although slightly less than that of the respective edges. Oxide layer that survived the cross-sectioning procedure was approximately 5–7 μm thick. The amount of billet material transferred to the front face was comparable to that on the front and rear

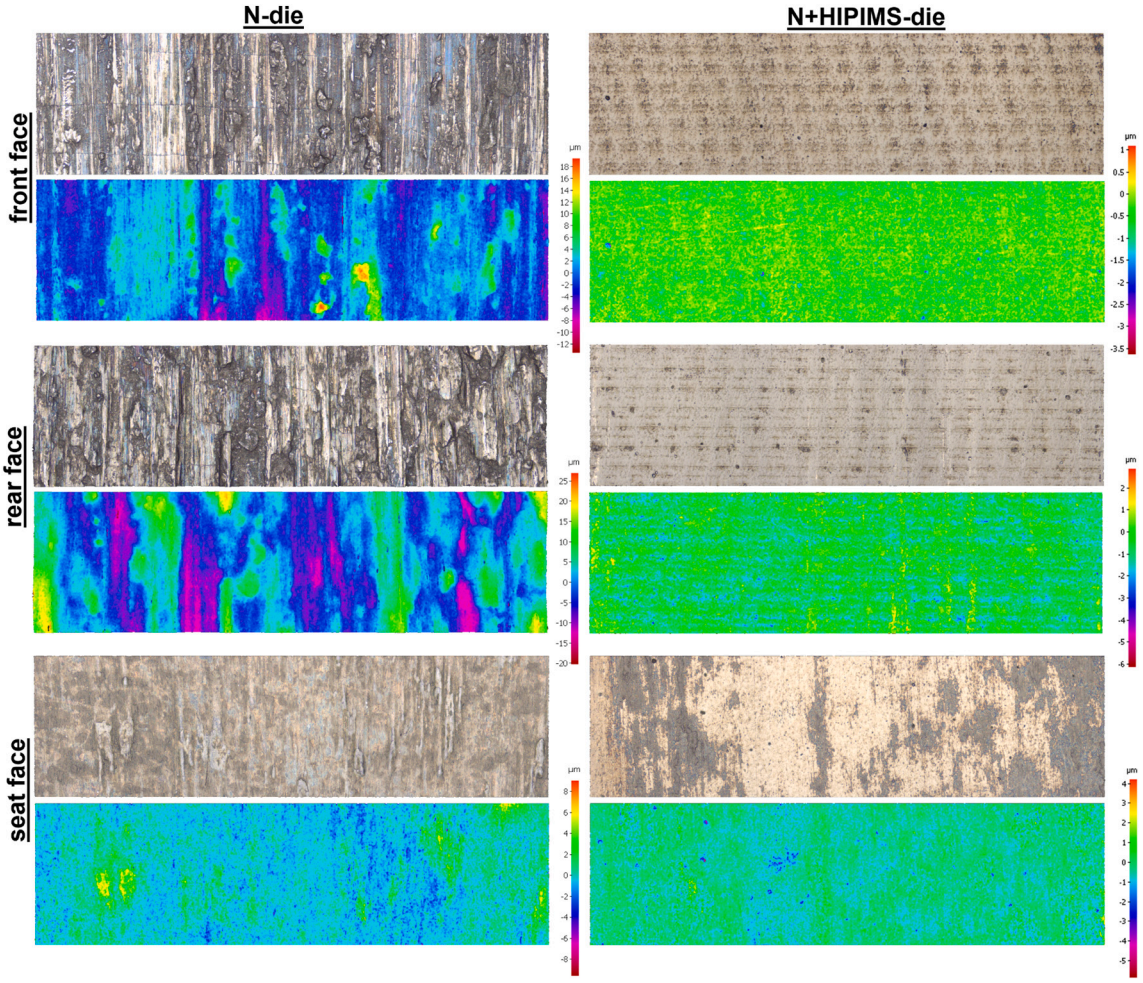

Fig. 9. True-colour and pseudo-colour optical profilometer images showing typical regions of the front, rear and seat faces of the post-forging N-die and N+HIPIMS-die. Image field dimensions are 3.94 × 1.09 mm.

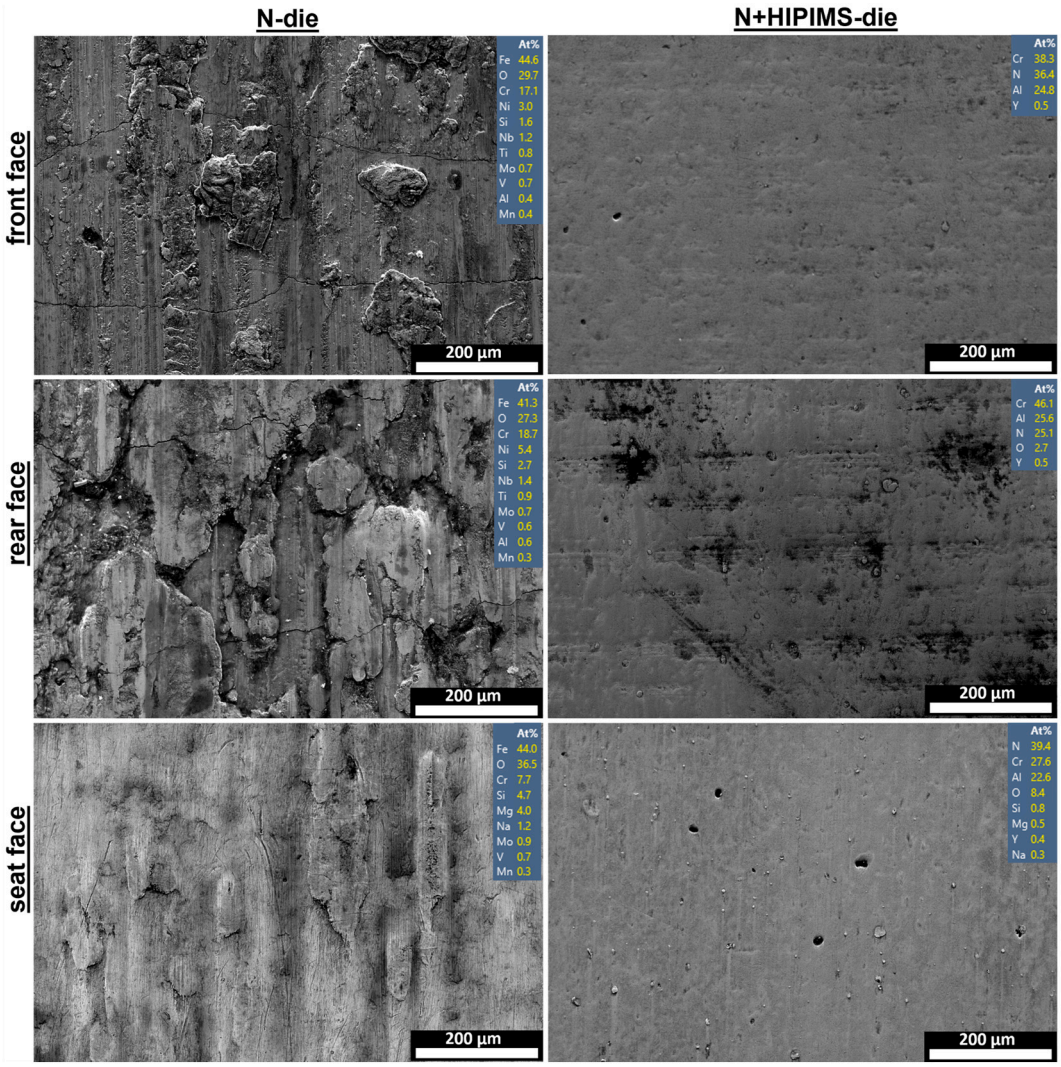

Fig. 10. SEM secondary electron images showing the typical surface of the front, rear and seat faces of the post-forging N-die and N+HIPIMS-die. The insets are the EDS determined elemental compositions.

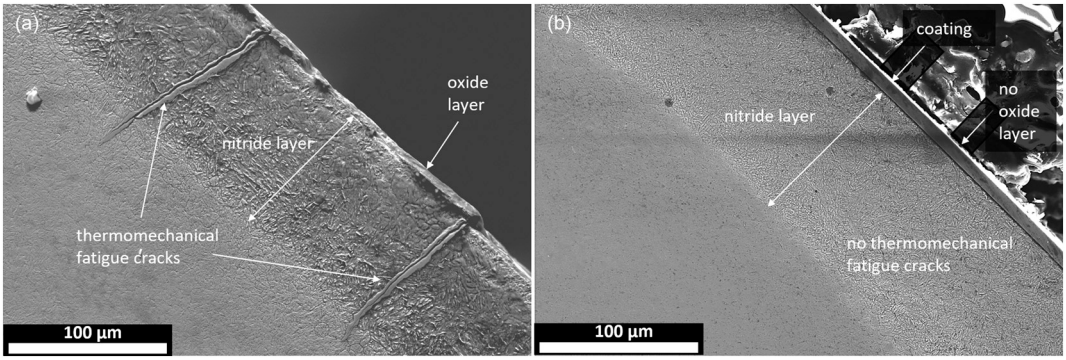

Fig. 11. SEM secondary electron images showing a typical region of the cross-section of the post-forging front face of the (a) N-die and (b) N+HIPIMS-die. Note that the difference in appearance of the nitride layer between specimens is due to etching variance. For the N-die, the rear face and extremities of the seat face were equivalent to that shown in (a). For the N+HIPIMS-die, the rear face and seat face were equivalent to that shown in (b).

edges. Pick-up on the rear face was significantly greater, with 5–9 at.% nickel consistently detected.

Scratches were widespread over the N-die seat face. TMF cracking and spallation occurred at the extremities only, consistent with where temperatures and stresses were greatest. Also commonplace over this face were longitudinally orientated elongated features that protruded approximately 10 µm above the surface plane. These were rich in chromium and oxygen and were thus products of die oxidation. At 30–40 at.%, the oxygen levels at this face were greater than the other N-die faces; however, this is misleading in terms of extent of oxidation

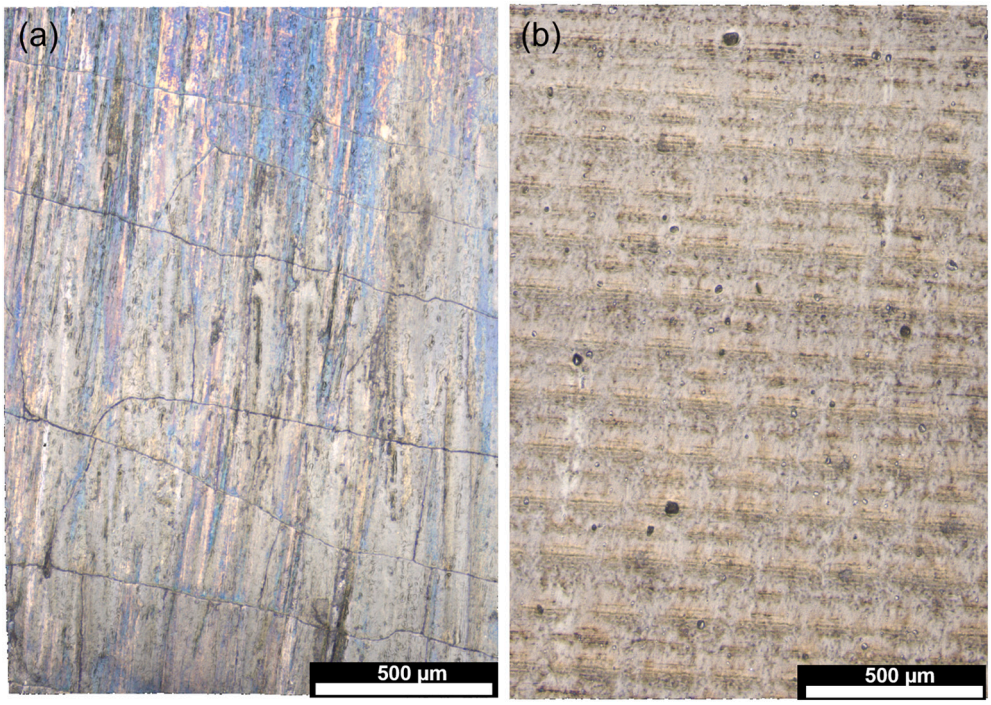

Fig. 12. True-colour optical profilometer images showing (a) the network of TMF cracks that formed on the front and rear faces of the N-die, and (b) the absence of such cracks on the faces of the N+HIPIMS-die. Image field dimensions are 1.43 × 1.99 mm.

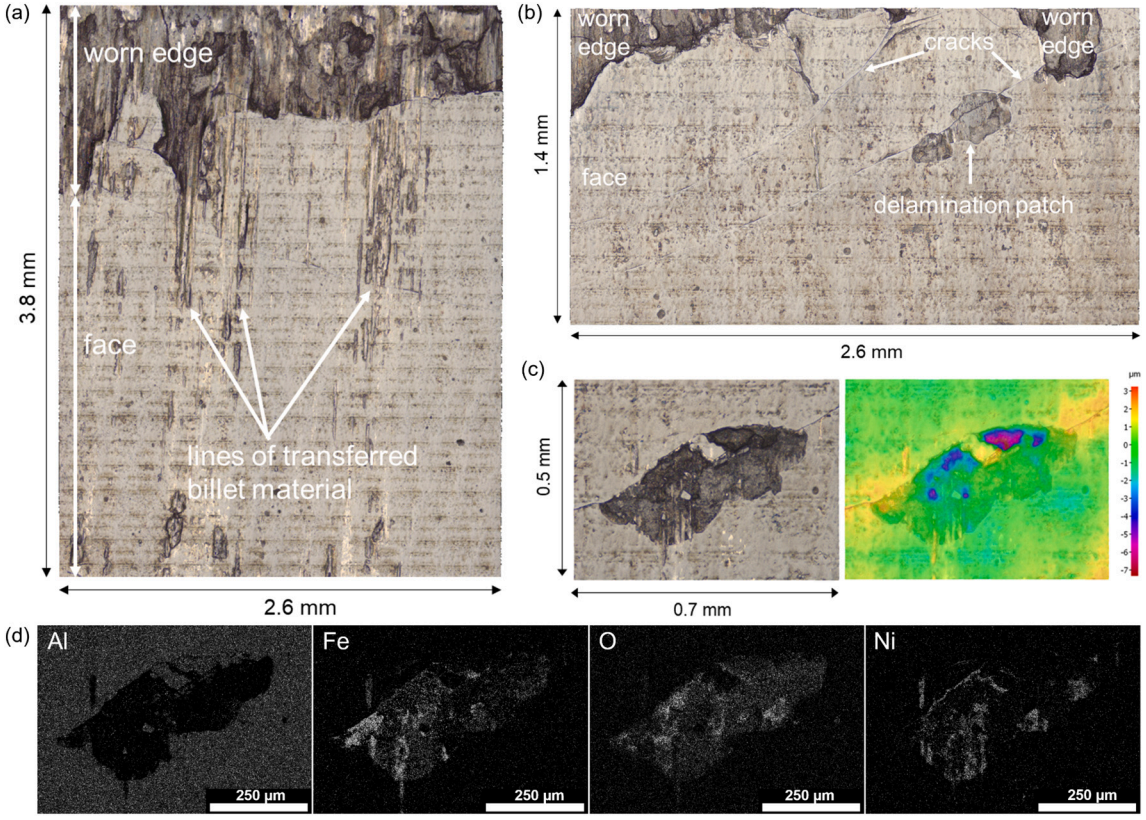

Fig. 13. Optical profilometry images from regions of the N+HIPIMS-die rear face near to the worn edge: (a) true colour image showing the most pronounced occurrence of the vertically orientated lines of raised material; (b) true colour image showing examples of cracks and a region of coating loss; (c) true colour and pseudo colour overlay images showing the largest region of coating loss; (d) shows aluminium, iron, oxygen, and nickel EDS maps of the region in (c).

because the amount of Si/Mg/Na/O containing contaminants was the highest of all regions of both dies. No elements indicative of pick-up were detected on this face.

In stark contrast to the N-die, neither abrasion marks nor TMF cracks were present on any of the N+HIPIMS-die faces. Indeed, that the superficial polishing texture was still clear over the front and rear faces (Figs. 9 and 12(b)) illustrates just how unaffected these regions were by the forging process. No oxygen was detected at the front face. The near-surface oxygen levels of the rear face were slight, i.e. 2–3 at.%. At 5–10 at.%, that of the seat face was highest; however, elements associated with the surface contamination described above in relation to other regions were also detected. That no oxide layers were apparent from cross-section analysis reveals that the oxygen content was confined to the uppermost near-surface region only. No billet material was detected on the front face or the seat face. The rear face was in general also free from pick-up, except for where the faint, vertically orientated lines that were noted in the macroscale observations occurred. EDS revealed these features to have the composition of IN718. Optical profilometry revealed them to be fragmented with total lengths of up to ≈3 mm and heights of up to ≈8 μm (Fig. 13(a)). They appear to have originated from the jagged demarcation line where the worn edge met the coated face, suggesting that material was sheared from the billet during siding. Curiously, however, they were not uniformly distributed but instead clustered off to one side of the face.

Although most of the rear face appeared essentially pristine, there were instances of coating damage near to the worn edge. Eight fine cracks had propagated to various extents from the boundary, seemingly convergent on a region ≈1.5 mm down and towards the horizontal midpoint of the face (Fig. 13(b)). There were also five irregularly shaped patches where the coating had been either partially or entirely removed. This was evident from optical profilometry that showed them to be just below the surface plane and EDS mapping that showed strong iron rather than aluminium signal (Fig. 13(c) and (d)). The smallest of these patches was <100 μm in all directions, and the largest had length ≈600 μm and breadth ≈200 μm. In all cases they were bisected or adjoined by one of the fine cracks, which supports mechanical fatigue cracking having been the precursor to coating loss at the rear edge. As further evidence of the coating being considerably more resistant to oxidation and pick-up than nitrided H13, oxygen and nickel signal counts were only appreciable where the substrate had been exposed.

3.3.3. Geometrical analysis

Fig. 14 shows a colour map of geometrical differences between the virgin N-die impression and the second-off billet; generated by inverting and fitting the GOM data from the former to that from the latter. Positive values indicate billet features that extend into plane of the die and negative values indicate those above the plane. Interpretation is complicated by the billet geometry having changed upon cooling due to thermal contraction. However, from knowledge that the die faces did not plastically deform during the run, positive deviations across faces can be attributed to thermal contraction. In contrast, we know from the good agreement between measurements of edge and corner sites from the post-forging dies and corresponding last-off billets (Fig. 16) that the geometries at these regions did not significantly change upon cooling. It thus follows that positive values at these regions would indicate a local billet volume greater than a corresponding virgin die region, and hence occurrence of local die yield. That no such regions are present indicates that the die did not suffer plastic yield upon the first two strikes. Therefore, any subsequent geometrical changes must be due to wear or induced by thermal softening. It can also be inferred from this analysis that, initially at least, there was moderate underfill at the fillets which could be why no discernible damage occurred at these sites. Underfill may be prevented in a future design by increasing the fillet radius.

Images derived from GOM data and colour mapped according to height differences between the virgin and corresponding post-forging die conditions are shown in Fig. 15(a) and (b). Direct comparisons between the two surface treatments in terms of maximum local depths and total local volumes of material loss can be made from the accompanying column plots: Fig. 15(c) and (d), respectively. It is readily apparent that the N+HIPIMS-die underwent significantly less material loss in all regions according to both metrics. The differences in volume changes between systems were more pronounced than height differences. The reason for this is evident from the GOM 'difference' images, which show that the lateral extent of negative deviations was considerably more confined when the HIPIMS coating was present. This is particularly true at the corners, where damage on the N-die extended along the full length of each respective upper edge causing the worn regions to merge. Attention should be drawn to the front edge of the duplex-treated die. Deviations in this region were less than the vertical resolution of the instrument and within alignment error. Furthermore, the optical profilometry and SEM analysis presented in the preceding section revealed that the post-forging edge underwent no loss of curvature and that the coating was intact. Therefore, the geometrical deviations apparent from the GOM method are dismissed as not real.

The geometry of a forged billet is essentially a 'negative' of the die impression at that point in the run. Consequently, insight into how the shape of the die changed during the run may be gained from geometrical analysis of selected billets. The accuracy of this method when applied to this system was assessed by comparing maximum height and volume changes measured from each last-off billet with those from the corresponding die (Fig. 16). These values ranged from being in reasonable to almost perfect agreement.

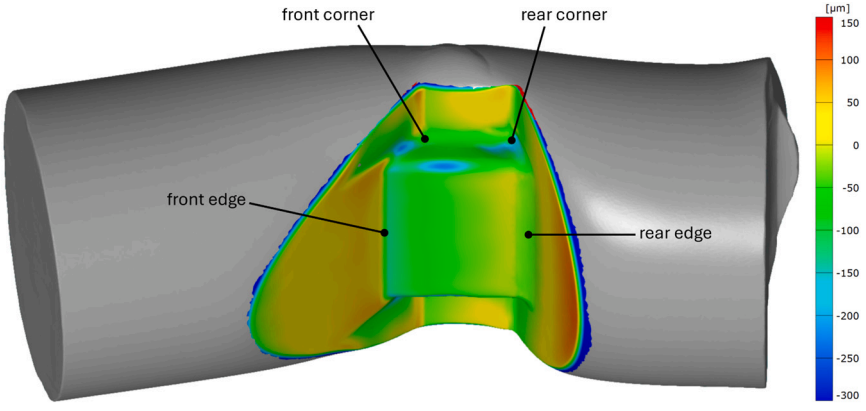

Fig. 14. Image derived from GOM data showing geometrical differences between the virgin N-die impression and the second-off billet. Positive values indicate billet features that extend into plane of the die and negative values indicate those above the plane. As discussed in the text, thermal contraction of the billet must be considered when interpreting these values.

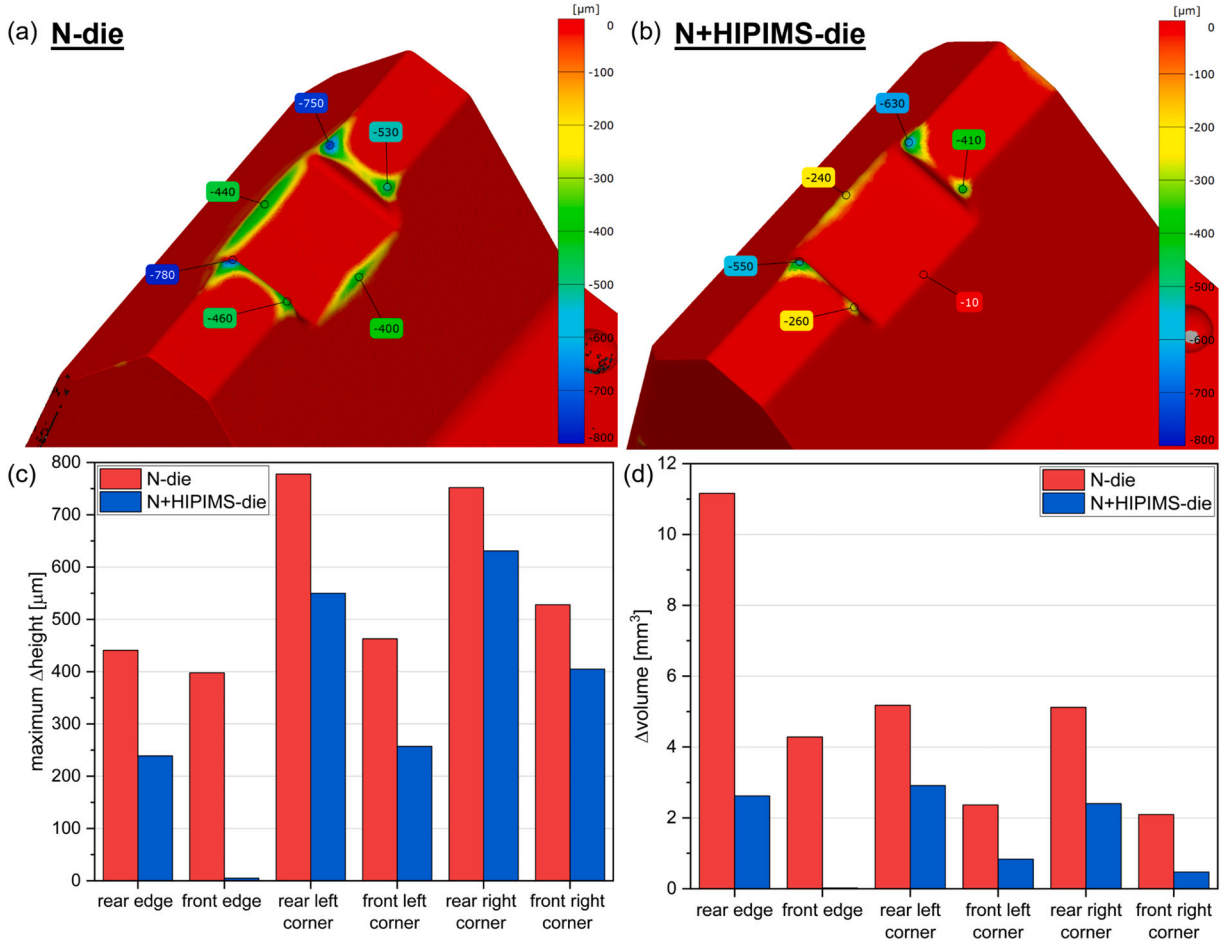

Fig. 15. (a) and (b) Images derived from GOM data showing how the post-forging geometry of the N-die and N+HIPIMS-die differed from the virgin condition. The annotations display the magnitude and position of the maximum depth of material loss at each of the two edge and four corner regions. (c) and (d) Column plots comparing the two surface treatments in terms of local maximum depths and volumes, respectively, of material loss.

GOM 'difference' images constructed from the first-off billet and each of the 50th, 100th, 150th, 200th and 260th -off billets are shown in Fig. 17(a). For the reasons given above when discussing the die 'difference' images, deviations at the region corresponding to the N+HIPIMS-die front edge are dismissed as not real. That the value stays constant over the course of the run further supports this conclusion. Similar reasoning also applies to the front corners of billets 50 and 100 and the rear edge of billet 50 forged on the N+HIPIMS-die.

Line plots of the highest positive deviation in each edge and corner region (Fig. 17(b)) reveal that the maximum depth of material loss from the front left corner of the N+HIPIMS-die after 260 forgings was less than that after 50 forgings on the N-die. At the rear edge, it was equivalent to after 50 forgings. At the front right and rear left corners, the post-forging N+HIPIMS-die was better in this respect than after 100 forgings on the N-die. At the rear right corner, it was equivalent to after 150 forgings.

An analogous plot of the billet volume data (Fig. 17(c)) indicates that at all die regions except the rear corners, the extent of volume loss from the N+HIPIMS-die after 260 forgings was superior to that from the N-die after 50 forgings. At the rear left and rear right corners, the final lost volumes were comparable to those after 50 and 100 forgings, respectively, in the absence of the HIPIMS coating. Of particular note is the front edge. Such was the extent of wear in this region of the N-die that the rate of loss tended towards a plateau after 200 forgings. In contrast, with the duplex treatment no loss was detected, i.e. the coating perfectly protected the die.

3.3.4. *Surface texture analysis*

Surface texture is a measure of wear sustained by a surface, and the difference between the conditions of the two post-forging dies in terms of all four measured texture parameters is considerable (Fig. 18(a)–(d)). An even clearer appreciation of the effect that the HIPIMS coating had in terms of surface texture evolution may be gained by considering the extent of change of each face relative to the virgin surface (Fig. 18(e)). With the N-die, the greatest relative change in any parameter was by a factor of 53. This was in the maximum height on the rear face. In comparison, the change in this parameter on this face for the coated die was by a factor of 2. With the N+HIPIMS-die, the greatest relative change in any parameter was by a factor of 3. This was in the ten-point height on the seat face, and on the uncoated die this changed by a factor of 12. An alternative way of comprehending this data is to consider that the mean relative change of all parameters across all faces of the coated die was by a factor of 2. Without the coating, it was by a factor of 28.

With the N-die, the relative increase in all parameters was significantly greater for the rear face than for the front face, which was in turn significantly greater than for the seat face. This order can be explained by the extent of abrasion that occurred at each region. With the N+HIPIMS-die, differences between the three faces were considerably less pronounced. Nonetheless, the seat face surface texture changed the most, followed by the rear face, with the front face having been essentially stable. With no abrasion marks evident on any of these faces, it is pertinent that the order correlates with that of near-surface oxygen content. Thus, the greatest changes to the surface texture of the HIPIMS coating were a consequence of the formation of a very thin oxide layer

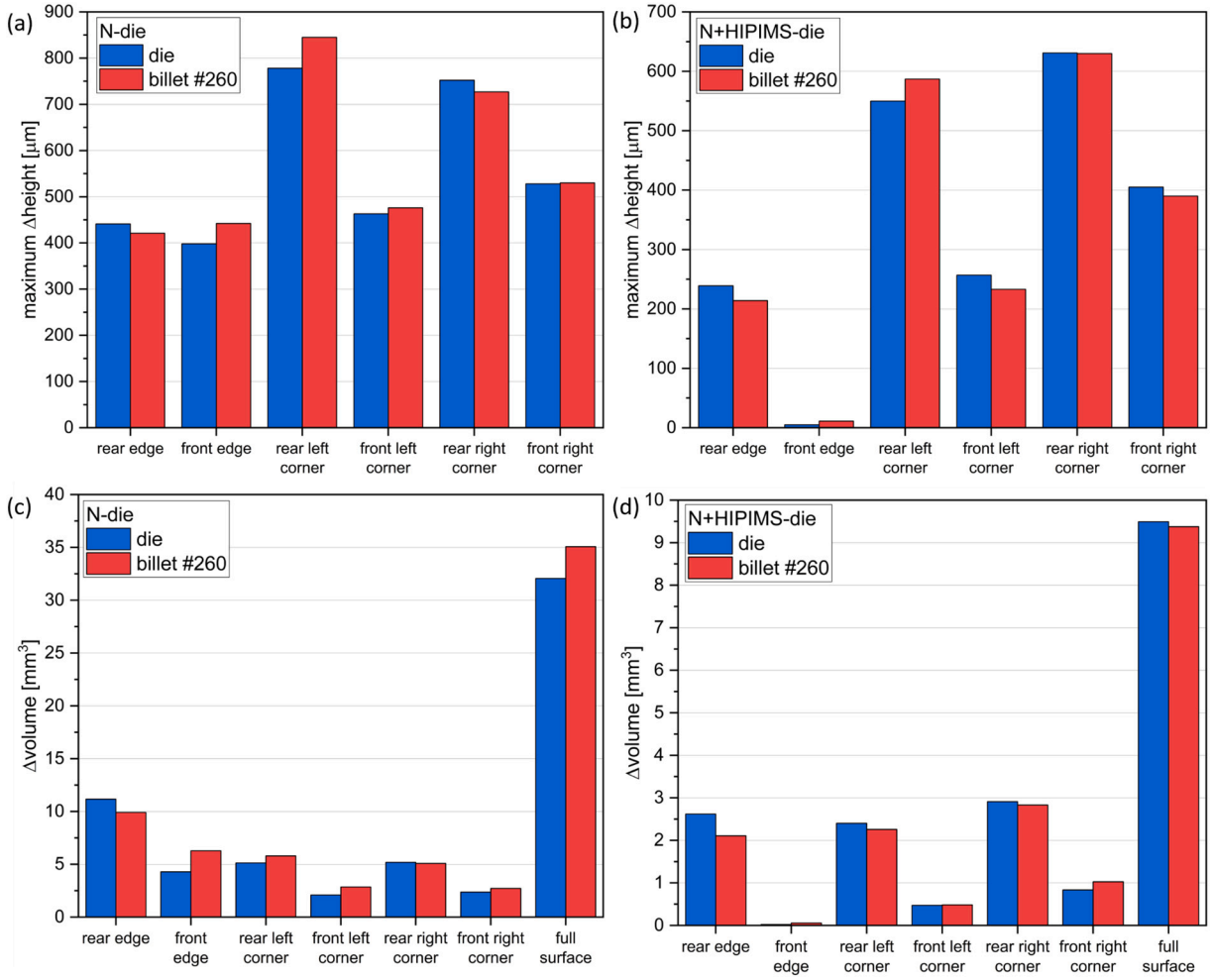

Fig. 16. Column plots comparing maximum height and volume change measurements from each post-forging die with those from the respective last-off billet.

rather than wear.

Of the four surface texture parameters considered here, the parameter Sdq is least reported upon in wear studies. This belies its potential importance, because friction is typically proportional to surface slope and also, for a larger slope the tendency for plastic deformation is greater [32]. Crucially, the HIPIMS coating provided pronounced protection against changes in surface slope. With the coated die, Sdq changes on all surfaces were by less than a factor of 2. In the absence of the coating, they were between 4 and 33.

3.3.5. *Microhardness*

Microhardness depth profile results from the N-die are shown in Fig. 19(a). These measurements were taken from a longitudinal cross section of the die that revealed the three faces and two edges but not the upper corners. In the virgin state, the nitride layer had a case depth of 105 ± 2 μm and a hardness maximum at the surface of 1180 ± 37 HK. For a nitrided die, a reduction in surface and near-surface hardness is typically a consequence of partial or complete displacement of the nitride layer and/or thermal softening. Considering first the front and rear edges, the measured hardness was below that of the bulk substrate for all distances evaluated. Thus, further to the nitride layer having been stripped in entirety, the substrate had been tempered to such an extent that at 400 μm the hardness was still below baseline level. As the case depth at the front and rear faces was reduced by just a slight or moderate amount, the significant drop in hardness exactly at the surface is attributed chiefly to thermal softening. At greater depths the hardness at the front face only slightly and for a short distance dropped below the bulk value, whilst that at the rear face the hardness was lower still and remained as such at the maximum depth it was measured. The hardness at the seat face was at the bulk level for all measured depths. As no abrasion occurred at this face and the nitride layer depth was equivalent to the virgin condition, this must have been caused solely by tempering.

Corresponding cross-section microhardness results from the N+HIPIMS-die are shown in Fig. 19(b). In the virgin state the coating had a hardness of 2921 ± 15 HK, and the case depth of the underlying nitride layer was 105 ± 4 μm. Considering first the regions where the coating and nitride layer remained intact post-forging. The hardness of the coating at the front face was equivalent to that in the virgin condition, whilst at the front edge, rear face and seat face it had reduced by amounts ranging from 4 to 12 %. However, any softening at these regions was seemingly confined to the coating, for microhardness measurements at depths coinciding with the nitride layer and bulk were consistent with those in the virgin condition. This reveals that where the coating survived the full forging run, it effectively and possibly even completely protected the substrate from thermal softening. Turning attention to the sole region where the coating was removed during the run for which microhardness depth profiles were obtained, i.e. the rear face. Consistent with other results indicating that after the abrasion protection of the coating was lost the nitride layer largely wore away, the mean hardness at the surface was just slightly greater than that of the bulk. Moreover, below this and until a depth of between 300 and 350 μm the hardness was lower than that of the bulk indicating that without the apparent thermal insulating effect of the coating, substrate tempering occurred also.

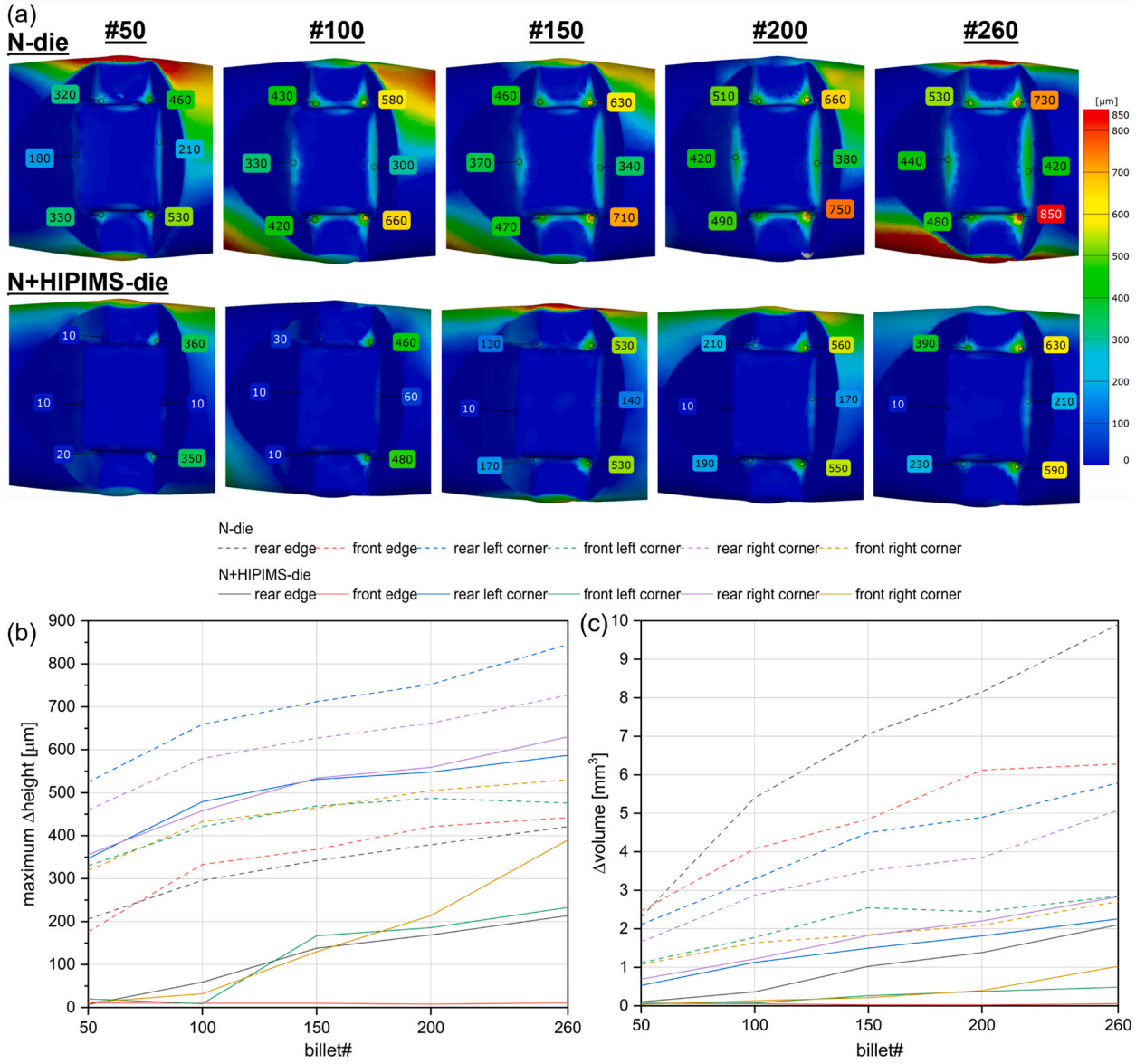

Fig. 17. (a) Images derived from GOM data showing how the geometry of selected forged billets differed from that of the first off. The annotations show the magnitude and position of the highest positive deviation in each edge and corner region. (b) and (c) are line plots showing the progressive changes in maximum heights and volumes, respectively, at these sites over the course of the run.

4. Discussion

A model die was designed to enable relatively low-cost quasi-industrial evaluation of the protection afforded by surface engineering technologies to hot forging dies. The aim was not to supplant production trials as this is the only method of achieving true validation due to thermomechanical stress magnitudes and distributions being highly process specific. The aim was rather to enable more realistic test conditions than can be achieved with laboratory-scale tribometers, thereby instilling greater industry confidence in findings which is an obstacle to technology uptake. Any evaluation method other than production trials will always entail a degree of abstraction and dampening of contact conditions. Considering this evaluation method, maximum surface temperatures in real-world closed die hot forging can range from 500 °C [33] to over 800 °C [34], and the FE simulation indicated that the setup employed here caused a maximum at the upper end of that range. Similarly, near-surface die stresses in a real-world press-based hot forging operation can reach approximately 1 GPa [33,35], and the maximum generated under these conditions was found to be reasonably comparable. Crucially, the accelerated test conditions enabled by the die design had the effect that just 260 billets were sufficient to induce in a nitrided H13 die many of the damage mechanisms that variously determine hot forging tool life in industry. Indeed, in terms of some of the mechanisms, degradation was considerable. It is thus reasonable to assert that via this method, useful insight may be gained into alternative surface engineering technologies by comparing a performance to that of a standard industrial practice.

In this work, the alternative surface engineering technology was a CrAlYN/CrN nanoscale multilayer HIPIMS coating deposited on a nitrided substrate, and it outperformed the nitrided only comparator in terms of all but one of the observed degradation mechanisms.

Widespread grooves in the direction of workpiece travel and an essentially steady rate of material loss indicate that abrasion was the wear mode behind the loss of curvature and eventual flattening of the front and rear edges of the N-die. Pronounced abrasion features were also present on the lower side adjoining faces. The HIPIMS coating was remarkably resistant to abrasion to the extent that no evidence of occurrence was detected on any region where the coating remained

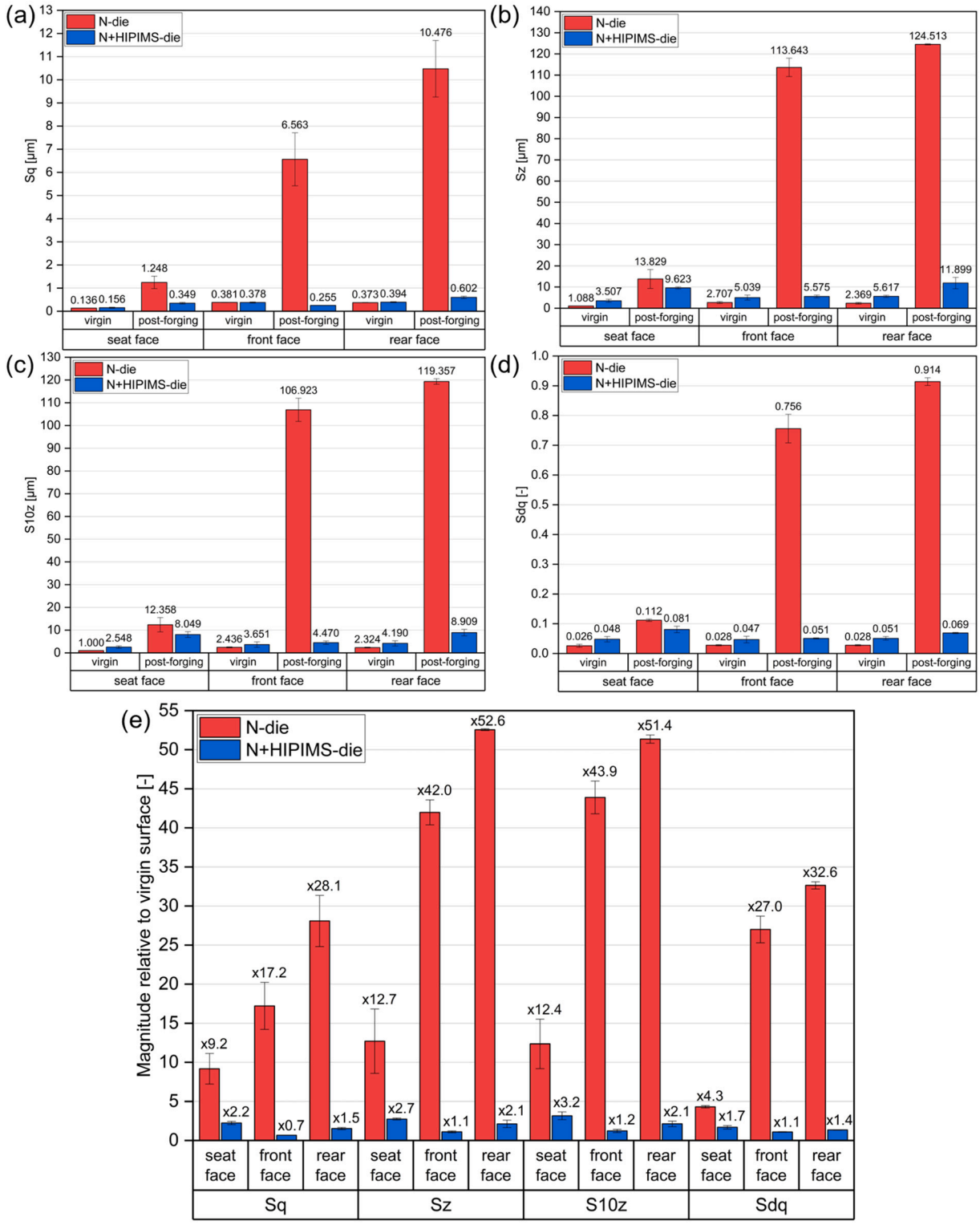

Fig. 18. Column charts showing (a)-(d) the surface texture of each face of the virgin and post-forging N-die and N+HIPIMS-die in terms of four areal texture parameters, Sq, Sz, S10z and Sdq; and (e) the surface texture evolution of each face in terms of the relative change of each of the four areal texture parameters. All values are the mean from three measurement areas and error bars represent one standard deviation.

post-forging. This aspect of performance can be explained by the super hardness of the coating [26], combined with the resistance to thermal softening observed in this work. The only region of the coated die that suffered abrasion was the rear edge, and it can reasonably be expected that this commenced only after local coating loss was complete.

In contrast, there was early and pronounced material loss at the rear corners of both dies. And the loss depth at the front corners of the N+HIPIMS-die exhibited sharp increases later in the run. This suggests that plastic yielding was, at least in the initial stages of damage, the dominant mode here. Despite the different mechanism, the coating still significantly reduced the extent of damage. The difference in loss depth and volume between the two systems was, depending on the corner,

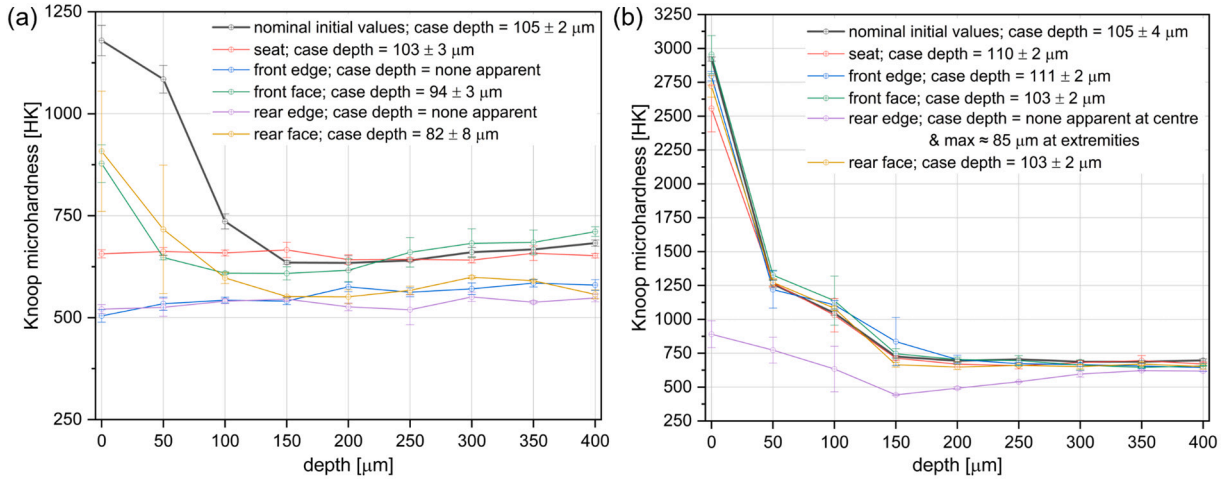

Fig. 19. Line plots showing Knoop microhardness measurements from the cross-section of the edge and face regions of the (a) N-die and (b) N+HIPIMS-die. All values are the mean of three measurements and error bars represent one standard deviation.

between 13 and 51 % and 44–83 %, respectively, less for the N+HIPIMS-die. Such a thin coating would not be expected to protect against pure yield, unless it somehow perturbed the underlying stress field. This, along with results indicating that the die did not inherently yield under the applied thermomechanical load, suggests that substrate softening was a prerequisite. However, microhardness measurements revealed this coating to provide excellent thermal protection to the substrate under these conditions. To know the mechanism for certain would require interrupted trials and a die geometry more conducive to analysis at such sites. In lieu of this and in accordance with the stress-raising characteristic of external corners, it is reasoned that the coating here cracked. Thereafter, the integrity of the insulating barrier would have been compromised and the substrate susceptible to tempering with subsequent cycles. It follows that final geometric differences here between the two systems were a combined consequence of a delayed onset and the substrate being only partially exposed. All this notwithstanding, of all the die regions these are of least industrial relevance because impressions seldom feature external corners because of reasons that include high susceptibility to yield.

The implication from the excellent thermal protection provided to the substrate under these conditions is that this CrAlYN/CrN HIPIMS coating had a low thermal conductivity. This is supported by results from single-layer, monolithic PVD coatings that found CrN to have a thermal conductivity of ≈2 $W\,m^{-1}\,K^{-1}$ and CrAlN ≈1.5 $W\,m^{-1}\,K^{-1}$ [36]. These values are over an order of magnitude lower than that of H13. Moreover, the nano-layered architecture can be expected to have reduced thermal conductivity further still due to a combination of the photon scattering effect of boundaries and the phonon scattering effect of local changes in layer density [37]. With the coating deposited for this study having been comparatively thick for PVD or HIPIMS, all these factors will have been enhanced.

The near-surface oxygen content of exposed H13 surface as measured via top-down analysis ranged from 25 to 40 %. That for the coating surface was 0–10 %. Furthermore, no coating oxide layer was evident from cross-section analyses, indicating that oxygen was confined to very top. Oxidation resistance under these conditions is consistent with previous work that found the temperature at which rapid oxidation of this coating in air commences to be between 950 and 980 °C [26]. Crucially, this aspect of performance will be replicated in real-world forging applications because although a die surface can temporarily reach a maximum of over 800 °C during a cycle [34], this occurs in the pressure phase during which exposure to atmospheric oxygen is cut off. Upon removal of the load, excess thermal energy rapidly dissipates into the bulk.

Such rapid surface heating and cooling coupled with mechanical loading and exacerbated by thermal shock when water-based graphite suspension is sprayed between forgings, can cause TMF cracking [38]. And this coating was evidently more resistant to TMF than a nitrided surface. A material is theoretically more durable with respect to cyclic thermal loading if it has (1) high thermal conductivity; thereby reducing the thermal gradient and, hence, differential thermal expansion, (2) high yield strength; reducing the amount of plastic deformation and, hence, tendency to initiate a crack, (3) low elastic modulus; reducing the amount of stress at a given thermal strain, and (4) low thermal expansion coefficient; reducing the amount of thermal strain. As has already been discussed, evidence indicates that this coating has a low thermal conductivity. Based on microhardness measurements, the room temperature yield strength was approximately 2 to 3 times that of the near-surface nitrided H13. However, the elastic modulus will also have been higher, albeit by a lesser relative amount i.e. a factor of <2 [39]. Finally, the thermal expansion coefficient is estimated based on sputter deposited CrN and CrAlN films to have been approximately two thirds that of the tool steel [40]. It is possible that the combination of the three favourable factors more than compensated for the low thermal conductivity and served to prevent TMF cracking. It is also probable that boundaries within the nanoscale multilayer architecture effectively arrested crack propagation in the event of initiation at the surface. Also of note in this respect is that CrN PVD coatings have been found to exhibit a certain resistance to thermal shock [16].

The other type of cracking observed was mechanical fatigue, and unlike TMF this affected both systems. Moreover, it was only observed at the same region of both dies, i.e. the rear edge. The effects were, however, more apparent with the duplex-treated die because this was the only edge or face of this system at which the coating was absent and the substrate sustained damage. Cracks penetrated the substrate and that they almost exactly spanned the region where the coating was absent indicates they were the principal contributory factor. When a crack initiates in a hard coating if it is not halted by an internal interface, it will either stop at the substrate interface, propagate along this interface, or propagate into the substrate [41]. Thus, once mechanical fatigue manifested either the coating delaminated or the loss of integrity rendered the coating susceptible to wear and it was removed in a more gradual manner. After the protection afforded by the superhard overlayer was gone, the die underwent abrasion in the same manner as the corresponding region of the uncoated die. That the maximum wear depth and volume at this edge of the N+HIPIMS-die were 46 % and 77 % less, respectively, than with the N-die is attributed to the delayed onset. Consequently, if the coated system could be made more resistant to

mechanical fatigue cracking, then the benefits to hot forging die life suggested by this work could be enhanced further.

Many studies have been performed to evaluate the mechanical fatigue behaviour of hard coating-ductile substrate systems, and conclusions vary as to whether the effect of the coating is positive or negative [42]. It has long been thought that for materials with a hardened surface layer, cracks tend to nucleate at the interface due to a significantly lower stress being required for a given plastic strain in the softer bulk [43]. More contemporary research, however, has explained the mechanism using the shear lag model which posits that the normal stress in the substrate is transferred to the coating due to the shear stress at the interface [44]. When the stress reaches the fracture stress of the brittle film, cracks nucleate from the surface and then propagate towards the interface. That cracks nucleate from the surface is well established for many materials and is because 1) stresses are higher near the surface and hence so is the concentration of plastic deformation and 2) asymmetric surroundings render near surface volumes subject to lower constraint [43]. Thereafter, if the propagating crack attains sufficient velocity, it will penetrate and fracture the substrate. Indeed, it has been found that the crack velocity in coatings that fracture in a brittle fashion can be so high that it "tremendously affects" the underlying substrate [44]. It is thus possible that this is the reason that the fatigue cracks in the substrate rear edge were distinctly broader for the N+HIPIMS-die than the N-die. Alternatively, it could have been that where cracks initiated a short distance from each other, they interacted at the substrate interface before coalescing and propagating into the bulk with an augmented stress intensity factor [45]. This could also explain why the cracks in the substrate of the coated system were less concentrated as well as broader.

Considering that crack nucleation is promoted by the presence of stress concentrators such as relatively sharp surface features, inclusions, and voids, this HIPIMS coating should in theory be somewhat resistant. Texture analysis (Figs. 4 and 18) found the surface to be smooth and extremely resistant to plastic strain; a dense columnar structure and nanolayer architecture are known to delay crack initiation and propagation, respectively; and the HIPIMS technique produces coatings with no droplet inclusions and minimal microstructural defects. In addition, HIPIMS-pretreatment provides high adhesion strength due to the implantation of metal into the substrate and efficient removal of contaminants. By way of example, low-cycle fatigue testing at 650 °C [46] and room temperature rotating beam fatigue testing [47] have found that a CrN/NbN nanoscale multilayer HIPIMS coating can improve the fatigue strength of the base material.

On the other hand, hard ceramic coatings possess limited intrinsic toughness and the virgin surface was punctuated by shallow depressions that are fairly common with PVD coatings. To improve this aspect of performance, an alternative die alloy composition [48] and/or heat-treatment [49] that improves toughness without sacrificing hardness may retard crack propagation into the bulk. Preferably, however, measures should be taken to prevent or delay crack initiation and propagation within the coating and improve adhesion. This could be achieved by optimising the thickness and residual stress in the coating and by reducing the bilayer thickness to increase the concentration of internal interfaces. A further route could be to introduce a toughness gradient through the thickness of the coating. This has been found to prevent crack propagation into a substrate by deflecting cracks in a direction parallel to the coating-substrate interface [50]. These potential improvements notwithstanding, it is the case that until such point the coating was lost, the substrate had been protected and the coating significantly delayed the onset of wear.

5. Conclusions

An accelerated method for evaluating the potential of surface treatments to protect hot forging dies was described that employs an industrial-scale press to forge small billets onto an impression. The motivation for developing this method was to enable more realistic test conditions than can be achieved with laboratory-scale tribometers whilst being reasonably low-cost and conducive to analysis. Ultimately, true validation can only be achieved by production trials, and it is hoped that surface treatments that are found to perform better than those currently in use according to this test may be deemed sufficiently derisked to warrant trials under real production conditions.

Industrial forging processes can require thousands of parts before die life becomes an issue, which hinders realistic ex situ testing and consequently uptake of novel damage resistant technologies. This accelerated quasi-industrial test was thus devised to simulate this phenomenon using a more economical number of billets. To achieve this, the die was purposely designed and the billet material selected to increase susceptibility to surface degradation.

Forging 260 IN718 billets at 1000 °C in a screw press was sufficient to induce in a nitrided H13 die many of the damage mechanisms that variously determine hot forging tool life in industry. The faces and edges were heavily abraded, considerable volume loss occurred at all edges and external corners, networks of thermomechanical fatigue cracks were widespread, and localised mechanical fatigue cracking occurred. Furthermore, oxide layer formation and pick-up were not insignificant.

In contrast, a CrAlYN/CrN nanoscale multilayer HIPIMS coating deposited onto a nitrided H13 die and subjected to the same conditions did not suffer abrasive wear or thermomechanical fatigue cracking and was considerably more resistant to oxidation and pick-up. Additionally, the coating provided excellent thermal insulation of the substrate and, hence, protection against thermal softening-induced plastic yield. At certain regions, however, the coating cracked during the run and protection was thereafter lost. The first of these regions were external corners, where once the insulating layer was compromised the substrate was susceptible to thermal softening and yield. Despite this, volume loss at these regions at the end of the run variously ranged from 44 % to 83 % less than for the uncoated system. It also occurred at an edge, where mechanical fatigue led to local coating removal and cracks penetrated the substrate. This was the same edge affected by mechanical fatigue on the uncoated die. Once the protection afforded by the superhard overlayer was lost, the die underwent abrasion in the same manner as the corresponding region of the uncoated die. The delayed onset, however, meant that volume loss was reduced by 77 %.

Only with an increased number of forgings can the longer-term coating performance be known at the die regions that did not suffer damage or significant damage. However, the aim was not to determine the limits of the coated die, but to assess the level of protection offered with respect to a benchmark without requiring a prohibitively expensive number of billets.

Potential routes to improving the performance of the coated system by increasing mechanical fatigue resistance were discussed. This notwithstanding, it is believed that based on these results this CrAlYN/CrN nanoscale multilayer HIPIMS coating has shown sufficient promise and been adequately derisked to warrant production trials under similar conditions. With the nature of hot forging die damage mechanisms being strongly process dependent, testing under different conditions may be deemed necessary to evaluate potential suitability for other processes. This would be possible with the presented method because it offers flexibility of die angles and radii, materials, settings and press type to tailor stresses towards those of an operation of interest.

CRediT authorship contribution statement

Christopher Fleming: Writing – original draft, Supervision, Project administration, Methodology, Investigation, Funding acquisition, Formal analysis, Conceptualization, Writing – review & editing. **William Kerr:** Formal analysis. **Bhaskaran Krishnamurthy:** Formal analysis. **Liza Hall:** Investigation. **Arunprabhu Sugumaran:** Investigation. **Arutiun Ehiasarian:** Writing – review & editing, Supervision. **Papken Hovsepian:** Supervision, Funding acquisition, Conceptualization.

Declaration of competing interest

The authors declare that they have no known competing financial interests or personal relationships that could have appeared to influence the work reported in this paper.

Acknowledgements

The authors gratefully acknowledge the financial support provided by the UK High-Value Manufacturing Catapult and an Impact Fellowship awarded by the Sheffield Hallam University Higher Education Innovation Fund.

Gratitude is expressed to Jacqueline Schramm for performing tensile tests, Lee McGarry for operating the press; Michael Canavan for preparing engineering drawings; and Jim Foster and Leslie Cummings for manufacturing the die.

The late Prof. Papken Eh. Hovsepian is greatly acknowledged for his mentorship in designing and leadership in delivering this work.

References

[1] Altan T, Shirgaokar M. Advanced die materials and lubrication systems to reduce die wear in hot and warm forging. In: 27th forging industry technical conference and energy summit, Fort Worth, USA; 2007.
[2] Behrens BA, Bouguecha A, Lüken I, Mielke J, Bistron M. Tribology in hot forging. In: Hashmi S, Batalha GF, Van Tyne CJ, Yilbas B, editors. Comprehensive materials processing. Oxford: Elsevier; 2014. p. 211–34.
[3] Purandare Y, Ehiasarian A, Hovsepian PE. Deposition of nanoscale multilayer CrN/NbN physical vapor deposition coatings by high power impulse magnetron sputtering. J Vac Sci Technol A 2008;26:288–96.
[4] Kouznetsov V, Macák K, Schneider JM, Helmersson U, Petrov I. A novel pulsed magnetron sputter technique utilizing very high target power densities. Surf Coat Technol 1999;122:290–3.
[5] Gronostajski Z, Kaszuba M, Hawryluk M, Zwierzchowski M. A review of the degradation mechanisms of the hot forging tools. Arch Civ Mech Eng 2014;14:528–39.
[6] Hawryluk M, Gronostajski Z, Widomski P, Kaszuba M, Ziemba J, Smolik J. Influence of the application of a PN+ Cr/CrN hybrid layer on the improvement of the lifetime of hot forging tools. J Mater Process Technol 2018;258:226–38.
[7] Dubois A, Dubar M, Dubar L. Warm and hot upsetting sliding test: tribology of metal processes at high temperature. Procedia Eng 2014;81:1964–9.
[8] Dubois A, Dubar M, Debras C, Hermange K, Nivot C, Courtois C. New environmentally friendly coatings for hot forging tools. Surf Coat Technol 2018;344:342–52.
[9] Terčelj M, Panjan P, Urankar I, Fajfar P, Turk R. A newly designed laboratory hot forging test for evaluation of coated tool wear resistance. Surf Coat Technol 2006;200:3594–604.
[10] Persson A, Hogmark S, Bergström J. Thermal fatigue cracking of surface engineered hot work tool steels. Surf Coat Technol 2005;191:216–27.
[11] Berti G, Monti M. Thermo-mechanical fatigue life assessment of hot forging die steel. Fatigue Fract Eng Mater Struct 2005;28:1025–34.
[12] Paschke H, Yilkiran T, Lippold L, Brunotte K, Weber M, Braeuer G, et al. Adapted surface properties of hot forging tools using plasma technology for an effective wear reduction. Wear 2015;330:429–38.
[13] Bay N, Olsson DD, Andreasen JL. Lubricant test methods for sheet metal forming. Tribol Int 2008;41:844–53.
[14] Smolik J. The wear mechanism of hybrid layer "PN+ CrN" during the hot forging process, journal of achievements in materials and manufacturing. Engineering 2011;49:215–23.
[15] Paschke H, Stueber M, Ziebert C, Bistron M, Mayrhofer P. Composition, microstructure and mechanical properties of boron containing multilayer coatings for hot forming tools. Surf Coat Technol 2011;205:S24–8.
[16] Smolik J, Walkowicz J, Tacikowski J. Influence of the structure of the composite: 'nitrided layer/PVD coating'on the durability of tools for hot working. Surf Coat Technol 2000;125:134–40.
[17] Thomas A, El-Wahabi M, Cabrera J, Prado J. High temperature deformation of Inconel 718. J Mater Process Technol 2006;177:469–72.
[18] Bhambri Y, Sikka VK. Forging of heat-resistant alloys. In: Semiatin SL, editor. Metalworking: bulk forming. ASM International; 2005. p. 269–83.
[19] Paulonis DF, Schirra JJ. Alloy 718 at Pratt & Whitney-Historical perspective and future challenges. Superalloys 2001;718:13–23.
[20] Bhavsar RB, Collins A, Silverman S. Use of alloy 718 and 725 in oil and gas industry, minerals, metals and materials society/AIME. In: Superalloys 718, 625, 706 and various derivatives(USA); 2001. p. 47–55.
[21] Czerwiec T, Renevier N, Michel H. Low-temperature plasma-assisted nitriding. Surf Coat Technol 2000;131:267–77.
[22] Cruz M, Nachez L, Gomez B, Nosei L, Feugeas J, Staia M. Ion nitrided AISI H13 tool steel part I–microstructural aspects. Surf Eng 2006;22:359–66.
[23] Ehiasarian A, Wen J, Petrov I. Interface microstructure engineering by high power impulse magnetron sputtering for the enhancement of adhesion. J Appl Phys 2007;101:054301.
[24] Vidakis N, Antoniadis A, Bilalis N. The VDI 3198 indentation test evaluation of a reliable qualitative control for layered compounds. J Mater Process Technol 2003;143:481–5.
[25] Hovsepian PE, Ehiasarian AP, Braun R, Walker J, Du H. Novel CrAlYN/CrN nanoscale multilayer PVD coatings produced by the combined high power impulse magnetron sputtering/unbalanced magnetron sputtering technique for environmental protection of γ-TiAl alloys. Surf Coat Technol 2010;204:2702–8.
[26] Hovsepian PE, Reinhard C, Ehiasarian A. CrAlYN/CrN superlattice coatings deposited by the combined high power impulse magnetron sputtering/unbalanced magnetron sputtering technique. Surf Coat Technol 2006;201:4105–10.
[27] He B, Ding S, Shi Z. A comparison between profile and areal surface roughness parameters. Metrol Meas Syst 2021;28:413–38.
[28] Prasad Y, Rao K, Sasidhar S. Hot working guide: a compendium of processing maps. ASM Int; 2015. p. 445–53.
[29] Davey K, Bylya O, Krishnamurthy B. Exact and inexact scaled models for hot forging. Int J Solids Struct 2020;203:110–30.
[30] Jabłońska M. Effect of the conversion of the plastic deformation work to heat on the behaviour of TWIP steels: a review. Arch Civil Mech Eng 2023;23:135.
[31] Miquel B, Jean S, Le Roux S, Lamesle P, Rézaï-Aria F. Heat-checking of hot work tool steels. In: European structural integrity society. Elsevier; 2002. p. 185–93.
[32] Pawlus P, Reizer R, Wieczorowski M. Functional importance of surface texture parameters. Materials 2021;14:5326.
[33] Widomski P, Kaszuba M, Krawczyk J, Nowak B, Lange A, Sokołowski P, et al. Investigating the possibility of regenearation by hardfacing for forging tools based on analysis of tool working conditions and wear evaluationy. Arch Metall Mater 2022;67:1395–410.
[34] Lange K. Metal forming: Surface quality of products. In: Buschow KHJ, Cahn RW, Flemings MC, Ilschner B, Kramer EJ, Mahajan S, Veyssière P, editors. Encyclopedia of materials: Science and technology. Oxford: Elsevier; 2001. p. 5433–6.
[35] Kim Y-J, Choi C-H. A study on life estimation of hot forging die. Int J Precis Eng Manuf 2009;10:105–13.
[36] Samani M, Chen GC, Ding XZ, Zeng XT. Thermal conductivity of CrAlN and TiAlN coatings deposited by lateral rotating cathode arc. Key Eng Mater 2010;447:705–9.
[37] Nicholls JR, Lawson KJ, Johnstone A, Rickerby DS. Methods to reduce the thermal conductivity of EB-PVD TBCs. Surf Coat Technol 2002;151-152:383–91.
[38] Buchmayr B. Damage, lifetime, and repair of forging dies. BHM Berg-und Hüttenmännische Monatshefte 2017;162:88–93.
[39] Tromas C, Stinville JC, Templier C, Villechaise P. Hardness and elastic modulus gradients in plasma-nitrided 316L polycrystalline stainless steel investigated by nanoindentation tomography. Acta Mater 2012;60:1965–73.
[40] Bartosik M, Holec D, Apel D, Klaus M, Genzel C, Keckes J, et al. Thermal expansion of Ti-Al-N and Cr-Al-N coatings. Scr Mater 2017;127:182–5.
[41] Ye T, Suo Z, Evans AG. Thin film cracking and the roles of substrate and interface. Int J Solids Struct 1992;29:2639–48.
[42] Bai Y-Y, Gao J, Guo T, Gao K-W, Volinsky AA, Pang X-L. Review of the fatigue behavior of hard coating-ductile substrate systems. Int J Miner Metall Mater 2021;28:46–55.
[43] Lukáš P. Fatigue crack nucleation and microstructure. In: Fatigue and fracture. ASM International; 1996. p. 96–109.
[44] Guo T, Qiao L, Pang X, Volinsky AA. Brittle film-induced cracking of ductile substrates. Acta Mater 2015;99:273–80.
[45] Bai Y, Xi Y, Gao K, Yang H, Pang X, Yang X, et al. Brittle coating effects on fatigue cracks behavior in Ti alloys. Int J Fatigue 2019;125:432–9.
[46] Hovsepian PE, Ehiasarian AP, Purandare YP, Mayr P, Abstoss KG, Mosquera Feijoo M, et al. Novel HIPIMS deposited nanostructured CrN/NbN coatings for environmental protection of steam turbine components. J Alloys Compd 2018;746:583–93.
[47] Hovsepian PE, Ehiasarian AP, Purandare Y, Sugumaran AA, Marriott T, Khan I. Development of superlattice CrN/NbN coatings for joint replacements deposited by high power impulse magnetron sputtering. J Mater Sci Mater Med 2016;27:147.
[48] Nakahama S, Matsuda Y, Namiki K, Ozaki K. The development of high hardness and toughness matrix type high speed tool steels: DRMTM. DENKI-SEIKO (Electric Furnace Steel) 2005;76:279–86.
[49] Pérez M, Belzunce FJ. The effect of deep cryogenic treatments on the mechanical properties of an AISI H13 steel. Mater Sci Eng A 2015;624:32–40.
[50] Ma D, Harvey TJ, Wellman RG, Ehiasarian AP, Hovsepian PE, Sugumaran AA, et al. Cavitation erosion performance of CrAlYN/CrN nanoscale multilayer coatings deposited on Ti6Al4V by HIPIMS. J Alloys Compd 2019;788:719–28.